sustainability

MDPI

Article

Assessing Post-Earthquake Firefighting Capacity of Water Distribution Networks Considering Isolation Valve Operations

Xiang He [1,2,*], Hong Huang [2], Chao Zhang [1] and Tingxin Qin [1,*]

[1] China National Institute of Standardization, Beijing 100191, China
[2] School of Safety Science, Tsinghua University, Beijing 100084, China
* Correspondence: hexiang@cnis.ac.cn (X.H.); qintx@cnis.ac.cn (T.Q.)

Abstract

The firefighting capacity of water distribution networks following earthquakes is essential for achieving the Sustainable Development Goals on resilient infrastructure and sustainable communities. Isolating broken pipes to curb leakage can preserve water supply, but the effects of such operations on post-earthquake firefighting remain incompletely understood. Here, we develop an improved valve closure decision method for post-earthquake firefighting that balances leakage reduction with water transmission capacity. Using this method as a basis, we examine how ground motion intensity, domestic water curtailment, firefighting flow, the number and spatial distribution of fires, valve layout, and valve closure policy jointly affect firefighting. A case study on a benchmark network shows that the valve closure scheme generated by the decision method reduces leakage by about 60–75% under spatially dispersed fires and the $N-1$ valve layout. Compared with no isolation, it also raises delivered firefighting flow from under 20% to over 80% of the design value. On average, these schemes deliver flow 5–10% below the optimal scheme. Valve placement, however, has a strong influence: under the $N-2$ layout, alternative placements can alter delivered flow by 10–20%. Adverse conditions—widespread pipe leakage caused by strong ground motion, hydraulic overload from clustered fires or firefighting flow surges, and sharp pressure reductions at fire nodes in low-pressure zones owing to excessive flow or leakage—can prevent the schemes from improving firefighting flow. These findings indicate that effective firefighting requires a combination of rational valve placement and closure schemes with seismic retrofitting of pipes and fire hazard mitigation.

Keywords: water distribution networks; post-earthquake firefighting capacity; isolation valve system; valve-closure scheme; seismic resilience; sustainable infrastructure

Check for updates

Academic Editor: Mara Lombardi

Received: 25 August 2026
Revised: 20 October 2026
Accepted: 22 October 2026
Published: 26 October 2026

Copyright: © 2026 by the authors. Licensee MDPI, Basel, Switzerland. This article is an open access article distributed under the terms and conditions of the Creative Commons Attribution (CC BY) license.

1. Introduction

Building disaster-resilient infrastructure and cities is integral to the United Nations Sustainable Development Goals (SDGs) 9 and 11. The severe threats posed by earthquakes make seismic resilience a core concern in sustainable urban development [1]. Apart from damage to infrastructure and buildings, post-earthquake fires (PEFs) [2] often cause substantial secondary losses. For example, the 1906 San Francisco earthquake caused approximately USD 400 million in fire-related losses, accounting for 80% of total losses [3]; the 1923 Kanto earthquake saw fires spread across 36 km^2 and destroy approximately 450,000 houses [4]. Reducing PEF risk is therefore vital for enhancing seismic resilience. Alongside eliminating fire hazards (e.g., flammable material leaks) [5], strengthening the firefighting capacity of water distribution networks (WDNs) is essential for effective

fire suppression. WDNs are essentially the only reliable source of firefighting flow [6]. However, wide seismic damage often degrades water supply capacity, and insufficient firefighting flow leads fires to spread uncontrollably [7]. Given the central role of WDNs in post-earthquake response, their firefighting capacity requires detailed investigation.

Assessing post-earthquake WDN functionality has long been a major research focus. The Federal Emergency Management Agency [8] and the American Lifeline Alliance [9] provide damage-probability models and procedural guidance for evaluating seismic impacts on WDN infrastructure. Analysts typically apply Monte Carlo simulation to generate stochastic damage scenarios and then use hydraulic models to compute demand satisfaction, thereby estimating post-earthquake functionality [10–12]. This workflow has been implemented in widely used programs such as GIRAFFE [13], REVAS.NET [14], and WNTR [15], yielding a largely standardized assessment framework. Firefighting flows far exceed domestic demand and must satisfy stringent pressure requirements, thus placing greater demands on hydraulic capacity. Accordingly, this framework has been extended to improve post-earthquake firefighting capacity and to analyze the mechanisms that affect it. We define firefighting capacity as the extent to which available firefighting flow satisfies required firefighting flow [6]. Optimization approaches have been employed to preserve the capacity by improving seismic retrofit for pipes [16,17]. Analytical studies have identified several constraints on the capacity, including pipe damage rate [6,18], the characteristics of water demand and PEFs (e.g., domestic demand, ignition rate, required firefighting flow, and fire location [6]), fire clusters immediately after an earthquake [19], and tank levels [20]. These studies have deepened the understanding of post-earthquake firefighting capacity and its influencing factors, yet how isolating broken pipes using the isolation valve system (IVS) affects this capacity remains insufficiently addressed.

Isolating broken pipes to curb leakage can effectively restore pressure and preserve supply capacity [21,22]. Because valves are not typically installed at both ends of each pipe, the IVS partitions a WDN into segments, each comprising multiple pipes. Consequently, isolating a broken pipe requires shutting down all pipes within the same segment. This practice can disrupt trunk mains, with profound impacts on hydraulic performance and water quality [23]. Recent studies aimed at quantifying and managing these outcomes fall into two categories: (1) assessment of valve closure impacts and, on this basis, optimization of valve placement and identification of key valves or segments, and (2) development of valve closure schemes for emergency responses. Assessment studies combine graph-based metrics with hydraulic indicators to evaluate how pipe isolations affect supply capacity [24,25]. Optimization studies treat valve locations as decision variables and the number of valves as a constraint, with the objective of minimizing the impact of isolation during disruptive events [26,27]. Identifying critical valves or segments aims to direct retrofit resources toward components whose failure or isolation causes the greatest propagation of impacts, thereby enhancing system reliability cost-effectively [28,29]. Real-time isolation schemes determine which valves to close and the sequence of closure [30], and they combine these actions with pump-speed and pressure control [31–33] to maintain water supply under failure conditions.

Unlike domestic demand addressed in these studies, firefighting flow is much larger and subject to stringent pressure requirements, making it more vulnerable to pipe isolation. Isolation disrupts network loops and cuts off important pipes on which firefighting flow depends, thereby more readily interrupting flow to numerous hydrants [34,35]. Most studies focus on a single-pipe break, isolating it by closing all valves in its segment. However, earthquakes often cause numerous breaks, and such simple isolation would take far more pipes out of service. With insufficient or improperly located valves, post-earthquake serviceability drops sharply and the recovery process becomes more uncertain [36].

Zhang et al. [37] also found that improper isolation can interrupt water supply for firefighting and medical use during post-earthquake peak demand periods. To secure supply to firefighting and medical nodes, Li et al. [38] identified paths with the greatest transmission capacity from water sources to those nodes and, while preserving the connectivity of those paths, determined which broken pipes could be isolated. They assigned smaller weights to pipes with larger transmission capacity and determined these paths using a Dijkstra's algorithm. This approach identifies pipes to be isolated within 20 s of computation, meeting the 48 h post-earthquake response requirement. However, requiring full connectivity of the highest-capacity paths prevents isolating broken pipes whose segments overlap those paths, potentially leaving some leaks inadequately controlled and thus limiting gains in firefighting flow.

To address this limitation, one feasible approach is to avoid enforcing full connectivity of the highest-capacity paths and instead modestly reduce the capacity to isolate additional pipe breaks, thereby limiting leakage while largely preserving water delivery. It is also important to recognize that a WDN's firefighting capacity is governed by multiple constraints. Under extensive seismic damage with multiple simultaneous fires, it remains unclear under what conditions this scheme can increase firefighting flow. We tackle these two problems and make two main contributions:

(1) Building on the method proposed in [38], we introduce an adjustable mechanism that relaxes the requirement for full connectivity along highest-capacity paths. The mechanism allows a controlled reduction in transmission capacity from water sources to fire nodes to isolate a larger set of broken pipes and thereby reduce leakage more effectively. By analyzing how firefighting capacity responds to different levels of capacity reduction, decision-makers can choose the isolation scheme that best meets their objectives.

(2) We integrate the improved valve closure decision method into a comprehensive analytical framework to examine how ground motion intensity, domestic water consumption, firefighting flow, the number and spatial distribution of PEFs, valve layout, and the relaxation mechanism in the valve closure scheme jointly influence firefighting capacity. Applied to a benchmark WDN, we quantify the resulting changes.

2. Method

2.1. Overview

Figure 1 summarizes the proposed method, whose main body comprises three modules detailed in Sections 2.2–2.5.

The first module generates seismic damage scenarios for the WDN and PEF scenarios. Seismic damage realizations are sampled from seismic fragility models to represent component failure states in WDNs. PEF scenarios are sampled from ignition models to capture the spatial distribution of fires and the associated firefighting-demand patterns. These two scenario sets are paired to generate a seismic damage–firefighting scenario ensemble. Both scenario types are simulated in WNTR 1.5.0 [39], which employs the EPANET 2.2.0 simulation engine [40].

The second module establishes a valve closure decision method. After mapping the relationships among pipes, segments, and isolation valves, we compute the flow contribution of each water source to every fire node and the hydraulic resistance from sources to fire nodes. We then combine these two measures to define each fire node's flow availability. Valve closures are constrained so that the resulting reduction in flow availability remains within an acceptable range, thereby limiting their impact on firefighting flow.

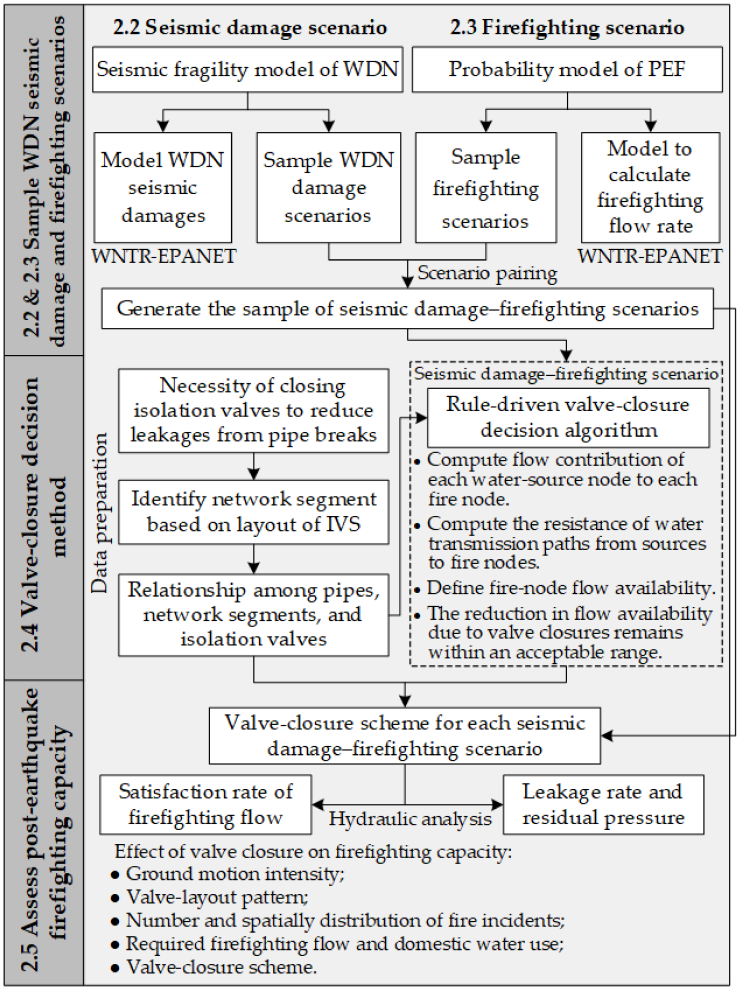


Figure 1. Method framework.

The third module proposes a framework for assessing a WDN's firefighting capacity. For each seismic damage–firefighting scenario, we generate a valve closure scheme and then perform a pressure-driven analysis [41] to compute available firefighting flow at each fire node. The firefighting capacity is quantified by the firefighting flow satisfaction rate, defined as the ratio of available to required firefighting flow; leakage rate and pressure are applied to corroborate capacity gains from isolating pipe breaks. We further elucidate how multiple influencing factors jointly determine firefighting capacity.

2.2. Modeling WDN Seismic Damage Scenarios

Seismic fragility models [9] fitted to historical damage data provide empirical probabilities that facilities will reach specific damage states under a given ground motion intensity. Buried pipes traverse wide areas and varied site conditions, so they often cross seismically unfavorable zones. Retrofitting pipes is generally harder and costlier than retrofitting localized facilities (e.g., water treatment plants). Historical records also show that pipe damage occurs far more often than damage to other components [42]. Therefore, this study focuses on pipe fragility to simplify scenario generation while preserving the dominant contributor to post-earthquake supply loss. Valve failures are excluded because assessing valve-closure schemes and layout effects requires a functioning IVS, and including valve failures would add complexity that confounds the analysis.

Seismic damage in pipes is classified as either breaks or leaks, and the probability of each mode depends on whether permanent ground deformation occurs [8]. For instance, if no permanent ground deformation occurs, breaks account for 20% of damage cases and

leaks for 80%; thus, their probabilities are 0.2 and 0.8, respectively. Schematic diagrams of pipe damage are shown in Figure 2a,b, where q^{leak} denotes the leakage rate (m^3/s). A break severs the pipe and stops flow, whereas a leak leaves the pipe partially functional. Figure 2c,d present the EPANET models for calculating q^{leak}. The parameter settings of the virtual node (VN), check valve (CV), and virtual reservoir (VR) are detailed in [43], and the method to calculate q^{leak} is provided in [13]. Each damage point is modeled as a VN. For breaks, CVs on both sides prevent flow through this pipe. VN links to VR via a virtual pipe that conveys the leakage flow. The pipe is assigned a minor loss coefficient of 1.0 and an infinite roughness coefficient, so head loss is attributed to the minor loss. A CV prevents reverse flow when pressure is negative. The leakage rate from a break, $q_{\text{B}}^{\text{leak}}$, and that from a leak, $q_{\text{L}}^{\text{leak}}$, are respectively defined as follows [13,15]:

$$q_{\text{B}}^{\text{leak}} = \frac{\pi D^2}{4}\sqrt{2g(P_{\text{VN}} - P_{\text{VR}})}, \tag{1}$$

$$q_{\text{L}}^{\text{leak}} = A_{\text{L}} \cdot \sqrt{2g(P_{\text{VN}} - P_{\text{VR}})}, \tag{2}$$

where D is the pipe diameter, g is gravitational acceleration (m/s^2), P_{VR} and P_{VN} are the pressure heads (m) at VR and VN, respectively, and A_{L} is the leak area (m^2). As an example, Table 1 lists the A_{L} of common leak forms of ductile iron pipes [13].

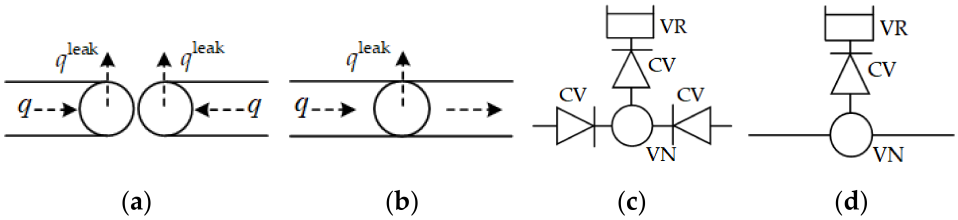


Figure 2. Schematic and simulation models of pipe seismic damage. Schematics of (**a**) breaks and (**b**) leaks. Simulation models of (**c**) breaks and (**d**) leaks.

Table 1. Probabilities and leak areas for ductile iron pipes.

Leak Form	Probability	Leak Area	Description
Circumferential joint loosening	0.8	$3\pi D$	D is pipe diameter (m);
Longitudinal cracking	0.1	$0.1L_{\text{C}}D$	L_{C} is longitudinal crack length
Pipe breach	0.1	$0.0025\pi D^2$	(m).

The distance from a pipe's start node to the k-th damage point, L_k, is defined as follows [13]:

$$L_k = L_{k-1} - \frac{\ln(1-\mu_{\text{L}})}{r_{\text{R}}},\ (L_k \le L,\ L_0 = 0), \tag{3}$$

where $\mu_{\text{L}} \in (0,1)$ is a uniform random number, L is the pipe length (m), and r_{R} is the repair rate. r_{R} represents the expected number of damage points per unit length of pipe and is defined as follows [44]:

$$r_{\text{R}} = C_{\text{R}} \times 2.88 \times 10^{-6} \times (980 \times pga - 100)^{1.97}, \tag{4}$$

where pga is the peak ground acceleration (in units of g); C_{R} is a correction coefficient accounting for pipe material, diameter, and geological conditions; 2.88×10^{-6} and 1.97 are regression coefficients fitted to damage data; 980 is the unit conversion factor between g and cm/s^2; and 100 is the threshold acceleration below which damage is assumed negligible. A seismic damage scenario is generated using the following steps:

Step 1. Calculate r_{R} for each pipe using Equation (4).

Step 2. Select one pipe and initialize the counter $k = 1$. Generate a random number μ_L and calculate L_k using Equation (3). If $L_k < L$, generate the k-th damage point, let $k = k + 1$, and repeat the process until $L_k \geq L$.

Step 3. For each damage point, generate a random number $\mu_1 \in (0, 1)$. If $\mu_1 > 0.8$, construct the break model at this point. Otherwise, construct the leak model at this point and generate another random number $\mu_2 \in (0, 1)$ to determine the leak form. For ductile iron pipes, for example, the forms are circumferential joint loosening, longitudinal cracking, and pipe breach when $\mu_2 \leq 0.8$, $0.8 < \mu_2 \leq 0.9$, and $\mu_2 \geq 0.9$, respectively.

Repeating this process N_S times yields a sample of seismic damage scenarios.

2.3. Modeling Post-Earthquake Firefighting Scenarios

Firefighting scenarios are characterized by the timing and location of PEFs. Historical data indicate that the highest incidence of fires occurs during the first few hours after the main shock, accounting for about 20% of all PEFs [8]. Because firefighting typically continues for at least 2–6 h [15,37], fires that ignite within this interval can overlap temporally. Such overlapping incidents severely strain a WDN's firefighting capacity, making them a critical and conservative scenario for capacity assessment [6,19]. Accordingly, we evaluate firefighting capacity under multiple-fire conditions. We use a static ignition model [45] to estimate the mean number of PEFs, N_{fire}, as follows:

$$N_{\text{fire}} = r_I \cdot A_F, \tag{5}$$

$$r_I = 0.0042 + 0.5985 \cdot pga, \tag{6}$$

where A_F is the total building area (10^5 m^2), and r_I is the ignition rate. The nodal probability of ignition depends on factors such as building density and the presence of combustible materials. In the absence of this data, $N_F = 0.2N_{\text{fire}}$ nodes are randomly sampled from the full set to generate one scenario, and this process is repeated N_S times to yield a scenario set. This stochastic sampling denotes fire occurrence under general conditions.

The spatial distribution of fire nodes influences whether required firefighting flows can be met. Nodes located far from water sources typically have limited pressure margins, and additional head losses from leaks often prevent the required flows [6,18]. By contrast, nodes with sufficient pressure are more resilient to these adverse effects. Accordingly, we use a stress test to assess the effects of placing N_F fire nodes in pressure-sufficient versus pressure-deficient areas, which represent favorable and adverse firefighting scenarios, respectively. We identify pressure-sufficient and pressure-deficient nodes as follows:

Step 1. Generate a sample of seismic-damage scenarios for the WDN (see Section 2.2).

Step 2. For each scenario, designate each node in turn as the fire node and compute the firefighting flow satisfaction rate for that node across all scenarios (see Equation (10)).

Step 3. Classify nodes by their average firefighting flow satisfaction rates. Following the failure threshold used in [46], we adopt 0.6 to mark severe deficiencies in firefighting flow. Accordingly, nodes with satisfaction rates below 0.6 are labeled pressure-deficient, and those with rates above 0.8 are labeled pressure-sufficient.

Figure 3 presents the simulation model of firefighting flow using the method in [19]. The fire node is connected in series to an emitter (EM) through a flow control valve (FCV) and a CV. The FCV limits the firefighting flow q_i^{fire} (m^3/s) transmitted in the virtual pipe to the required flow Q_i^{fire} (m^3/s), and the CV prevents reverse flow resulting from negative pressure. The EM coefficient γ is set to 100 times Q_i^{fire}, and its elevation is set to the elevation of node i plus the required firefighting pressure P_{fire} (m) [40]. When the node's pressure P_i satisfies P_{fire}, $q_i^{\text{fire}} = \gamma \cdot (P_i - P_{\text{fire}})^{0.5}$; otherwise, $q_i^{\text{fire}} = 0$.

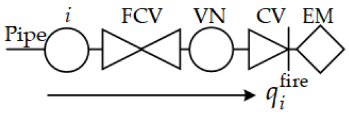


Figure 3. Simulation model of firefighting flows.

2.4. Valve Closure Decision Method

Figure 4 illustrates q^{leak} for different damage states in ductile iron pipes, calculated using the models in Section 2.2. Pipe diameters vary from 0.1 to 1.0 m, covering common sizes from distribution branches to transmission mains. Pressures of 5, 10, 15, and 20 m are representative values that span typical firefighting conditions from insufficient to adequate pressure. Leakage from a break increases more rapidly with pipe diameter, reaching 10–100 times the leakage of a comparably pressurized leak of the same diameter. This large outflow and its resulting pressure reduction underscore the importance of isolating pipe breaks to restore water supply capacity [30,37].

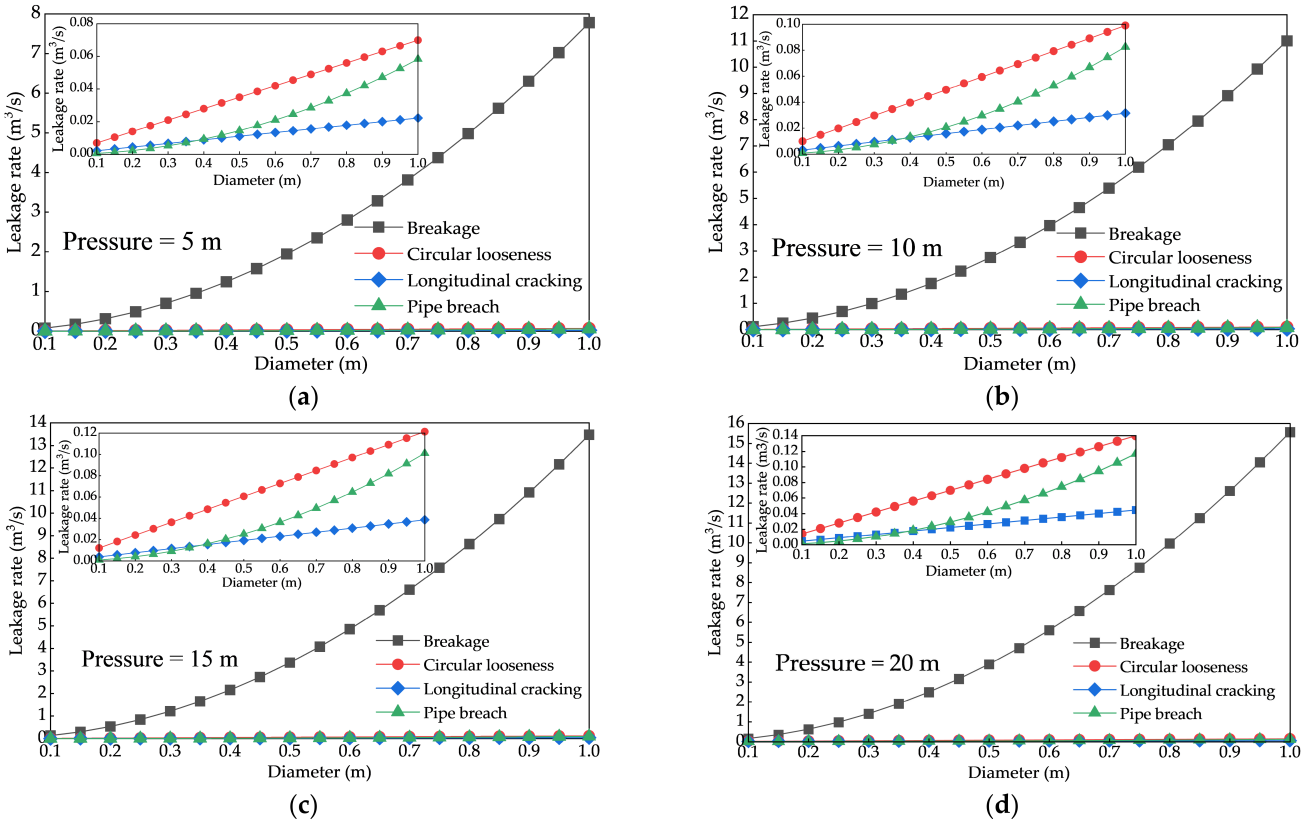


Figure 4. Leakage rates of damaged pipes under different failure types. (**a**) Pressure = 5 m. (**b**) Pressure = 10 m. (**c**) Pressure = 15 m. (**d**) Pressure = 20 m.

The algorithm defining relationships among segments, valves, and pipes is presented in [47]. The procedure for choosing which valves to close and for determining the resulting isolated segments is detailed in [21]. Because firefighting flow is computed on the residual WDN after isolation, the valve closure scheme reports the set of isolated pipes rather than closed valves. As shown in Figure 5, isolating the break on L11 severs L7, L10, and L14 and also isolates the downstream pipes L8, L12, and L15. Thus the scheme removes {L7, L8, L10, L11, L12, L14, L15} from the network before computing firefighting flow. To prevent such cascading isolation from obstructing required firefighting flows, valve closure schemes must balance leakage reduction against the impact of isolation. Therefore, we improve the valve closure decision method in [38] in two ways.

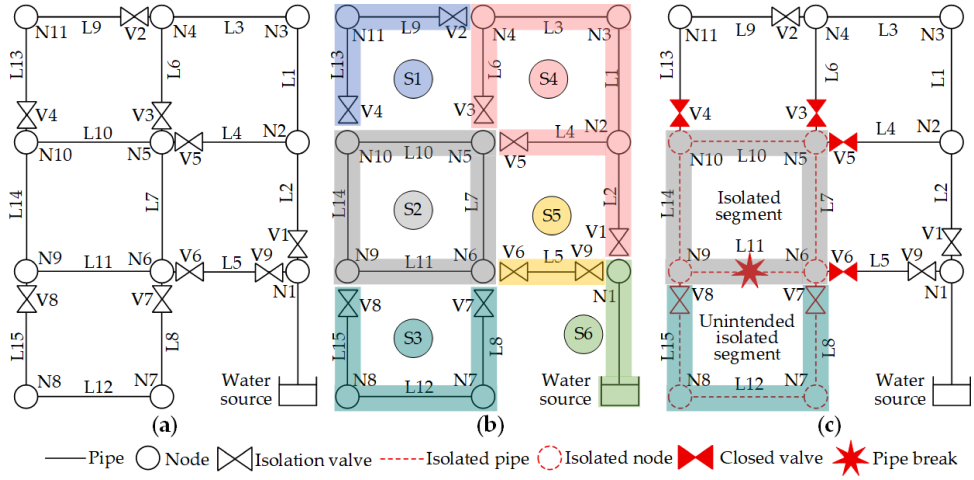


Figure 5. Schematic illustration of the pipe-isolation procedure: (**a**) valve placement; (**b**) segment division; (**c**) isolation of damaged pipes.

First, we replace flow with a Hazen–Williams (HW) resistance coefficient [40] to represent pipe transmission capacity. Reductions in domestic demand and increases in firefighting flow can change flow distribution, so using normal-condition flows to quantify capacity may understate post-earthquake transmission potential. Because flow preferentially follows the minimum-resistance paths from sources to nodes, we treat that path as the highest-capacity path. Looped WDNs transmit flow from source to fire nodes along multiple paths. K-shortest path algorithms [48] tend to yield paths that share a large portion of pipes and exhibit marginal differences in resistance, particularly when K is small. Consequently, they can neglect alternative paths that are largely independent of the shortest path but nonetheless offer high transmission capacity. To ensure both redundancy and substitutability, we therefore identify independent paths that retain relatively high transmission capacity.

Second, we introduce a relaxation threshold θ to represent the tolerance for reductions in transmission capacity. We select the closure scheme that meets the threshold and isolates the largest number of pipe breaks. If multiple schemes remain feasible, we choose the one that minimizes the reduction in transmission capacity.

Figure 6 shows the algorithmic procedure.

Step 1. For each fire node, construct a firefighting simulation model and apply tracer analysis to quantify the flow contribution of each water source. Denote the flow from source node s to fire node i as $q^{\text{fire}}_{s\to i}$; larger values indicate a greater contribution of s to i.

Step 2. Convert the WDN into an undirected, weighted graph G. Assign each edge a weight equal to the resistance coefficient, $10.67C^{-1.852}D^{-4.871}L$, where C, D, and L denote a pipe's roughness coefficient, diameter (m), and length (m), respectively. For each source–fire-node pair, we first find the shortest path and remove the edges along that path. We then identify the shortest path in the updated network and remove those edges, repeating this process until no source retains a path to the fire node. The equivalent resistance of these independent paths from s to i, $l_{s\to i}$, is defined as follows [49]:

$$l_{s\to i} = \left(\sum\nolimits_k l_{s\to i,k}^{-1/n}\right)^{-n},\ n = 1.852, \tag{7}$$

where $l_{s\to i,k}$ denotes the k-th high-capacity path from s to i.

Step 3. Let N_{break} and n_{close} ($N_{\text{break}} \geq n_{\text{close}} \geq 0$) represent the numbers of pipes with breaks (broken pipes) and of closed pipes, respectively. Let $n_{\text{close}} = N_{\text{break}}$ by prioritizing closure of all broken pipes to maximize leakage reduction.

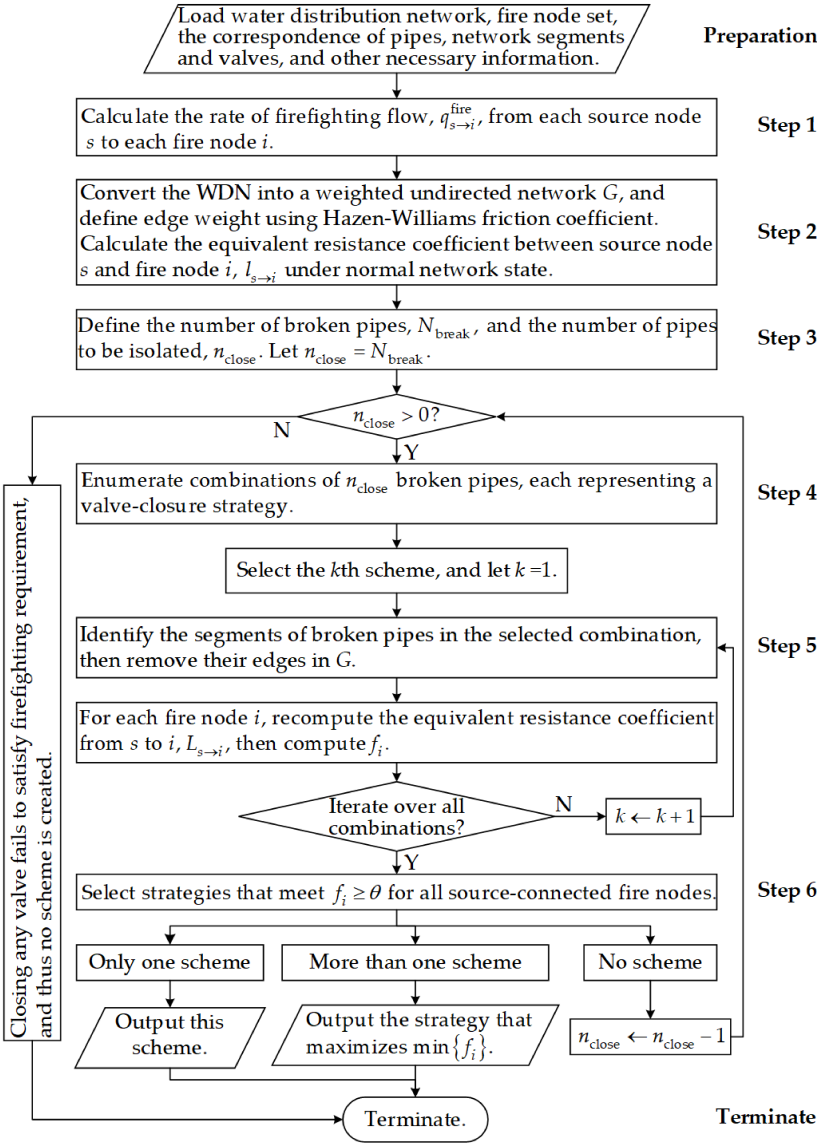


Figure 6. Valve closure decision procedure.

Step 4. If $n_{\text{close}} > 0$, enumerate combinations of n_{close} broken pipes; each combination represents a valve closure scheme. If $n_{\text{close}} > 0$, then proceed to Step 5; otherwise, no feasible scheme is produced, and the procedure terminates.

Step 5. For each combination in Step 4, identify pipes to be isolated and remove them from G. For each fire node i, recompute the equivalent resistance, $L_{s\to i}$, using the updated network. In the HW formula, $h_f \propto l_{i\to j} \cdot Q_{i\to j}^{1.852}$, indicates that the flow rate $Q_{i\to j}$ at a given head loss h_f is inversely proportional to the $1/1.852 \approx 0.54$ power of the resistance $l_{i\to j}$. Accordingly, the effect of isolation on the transmission capacity at node i is defined as

$$f_i = \sum_s w_{s\to i} \left(\frac{l_{s\to i}}{L_{s\to i}} \right)^{0.54}, \tag{8}$$

$$w_{s\to i} = \frac{q_{s\to i}^{\text{fire}}}{\sum_s q_{s\to i}^{\text{fire}}}, \tag{9}$$

where $w_{s\to i}$ denotes the relative contribution of s to i, and $l_{s\to i}/L_{s\to i}$ denotes the reduction in transmission capacity. Because $\sum w_{s\to i} = 1$ and $l_{s\to i,0}/l_{s\to i} \in (0,1]$, $f_i \in [0,1]$. f_i captures firefighting flow availability. Sources often contribute unevenly to the flow at a fire node. Valve closure that increases the resistance between the high-contribution source and the

node can reduce f_i and potentially prevent the node from receiving flow. Therefore, as f_i approaches 1.0, the likelihood of achieving sufficient flow increases. After examining all closure schemes and computing f_i for each fire node, proceed to Step 6.

Step 6. If all fire nodes connected to water sources satisfy $f \geq \theta$, the scheme is considered feasible. If multiple feasible schemes exist, compute $\min\{f_i\}$ for each and select the scheme that maximizes this value. Terminate the algorithm after producing the scheme. If no feasible scheme exists, set $n_{\text{close}} \leftarrow n_{\text{close}} - 1$ and return to Step 4. Since $f \in [0,1]$, it follows that $\theta \in [0,1]$. Across networks, ground-motion intensities, and fire scenarios, a given θ can correspond to different firefighting flows. As θ approaches 1.0, allowable increases in resistance are limited, fewer pipes are isolated, and the scheme becomes more conservative. Conversely, as θ approaches 0, more breaks are allowed to be isolated, but firefighting flow may diminish. Decision-makers should map firefighting flow against θ over [0, 1] to identify an appropriate θ interval.

Pipe breaks are readily detected because they produce marked hydraulic anomalies, whereas leaks are often hard to identify. Paez et al. [46] indicates that, for pipes under 300 mm, a leak typically remains undetected unless its rate reaches 2.5 L/s. Using these data, Zhang et al. [37] found that approximately half of pipe damage—primarily leaks—is detected only after a complete inspection 48 h post-earthquake. Consequently, during the first few hours when fires are most concentrated, decision-makers typically lack sufficient hydraulic information to produce schemes that maximize firefighting flow. The method from [38], as improved here, selects post-closure network states that remain close to normal operation. For each fire node, it prioritizes sources that contribute the most under normal conditions so those sources remain effective. In other words, closures should limit the reduction in transmission capacity from prioritized sources to the fire node within an acceptable range. Although a normal-condition baseline may not be optimal, it provides a practical alternative when post-earthquake hydraulic information is incomplete, and its minimal computational cost meets emergency-response timeliness requirements.

2.5. Assessment of Post-Earthquake Firefighting Capacity

2.5.1. Assessment Metrics

The assessment metrics include the firefighting flow satisfaction rate, the leakage rate, and the residual pressure. We use the average firefighting flow satisfaction rate at each fire node to quantify firefighting capacity. The average flow satisfaction rate $F_{i,\text{fire}}$ for fire node i across all scenarios is defined as

$$F_{i,\text{fire}} = \frac{1}{N_S} \sum_{s=1}^{N_S} \frac{q_{i,s}^{\text{fire}}}{Q_{i,s}^{\text{fire}}}, \tag{10}$$

where $q_{i,s}^{\text{fire}}$ and $Q_{i,s}^{\text{fire}}$ are the available and required firefighting flow (m^3/s) at node i in scenario s, respectively. The average satisfaction rate across all fire nodes, $\sum F_{i,\text{fire}}/N_{\text{fire}}$, is defined as the system firefighting capacity F_{fire}.

Examining the relationship between firefighting flow and leakage clarifies how valve closure enhances firefighting capacity. We use the leakage rate F_{leak} to quantify the effectiveness of leakage reduction:

$$F_{\text{leak}} = \frac{1}{N_S} \sum_{s=1}^{N_S} \sum_{i} q_{i,s}^{\text{leak}}, \tag{11}$$

where $q_{i,s}^{\text{leak}}$ is the leakage rate (m^3/s) at damage point i in scenario s. If point i is isolated, then $q_i^{\text{leak}} = 0$. As F_{leak} approaches 0, overall leakage reduction becomes more effective.

Excess flows for domestic and firefighting demands increase head loss, which lowers pressure and thus constrains available firefighting flow. We quantify pressure changes using the normalized residual pressure index $\overline{P}_i$, defined as

$$\overline{P}_i = \frac{P_{i,\text{res}}}{P_{i,0}}, \tag{12}$$

where $P_{i,\text{res}}$ and P_0 denote the pressure (m) at node i under damaged and normal conditions, respectively. The mean value of $\overline{P}_i$ across all nodes, $\overline{P}_{\text{sys}}$, reflects the network's ability to maintain pressure. Water curtailment and leakage reduction lower excess flow in the network, thereby reducing head loss and increasing $\overline{P}_{\text{sys}}$. Accordingly, $\overline{P}_{\text{sys}}$ captures the hydraulic improvement achieved by these two measures.

2.5.2. Sensitivity Analysis for Firefighting Capacity Drivers

The performance of these metrics depends on multiple intrinsic and external factors of a WDN. Based on prior studies [6,18], ground motion intensity, valve layout, domestic water curtailment, required firefighting flow, the number and spatial distribution of fires, and closure scheme are identified as the primary drivers. We apply sensitivity analysis to quantify the joint effects of these factors on firefighting. The underlying mechanisms and parameter settings for each factor are described below.

Ground motion intensity determines the extent of WDN damage. Leakage from damaged pipes fundamentally compromises a WDN's ability to deliver firefighting flow. We generate seismic damage scenarios across different *pga* values to examine this factor's influence on firefighting capacity.

Valve layout determines segment size and thus the probability that valve closure will interrupt water supply over large areas. We examine firefighting capacity across three layouts: N, $N-1$, and $N-2$ [47]. The N layout places valves at both ends of every pipe, making it an ideal layout for comparative analysis rather than a practice in real WDNs. The $N-1$ and $N-2$ layouts are more typical; they remove 1 or 2 valves per node, respectively, reducing installation and maintenance costs while retaining operational flexibility. Compared with random layouts, these strategic schemes produce a more uniform valve distribution given the same total number of valves.

Reasonable limits on domestic water use reduce network head loss, which improves pressure and is essential for maintaining post-earthquake supply [15]. Required domestic water is modeled as the base demand multiplied by a coefficient $\lambda \in [0,1]$; $\lambda = 0$ denotes complete curtailment of domestic water, while $\lambda = 1$ indicates no restriction. We examine the effect of water curtailment across a range of λ values.

Firefighting flow alters pressure by changing head loss and thus affects available firefighting flow. Environmental hazards, such as fire spread, can drive required firefighting flow above the design value. Here, we model required flow as the design flow multiplied by a coefficient $\mu \geq 1$; larger μ denotes greater required flow. We examine the required flow over a range of μ values.

The number of fire nodes determines the total firefighting flow required by the system. In low-pressure areas, available flow often falls short of demand, and clusters of fire nodes can depress local pressure and reduce supply. We therefore consider three fire scenarios: (1) stochastically distributed nodes representing general conditions; (2) nodes located in pressure-sufficient or -deficient areas to denote favorable and adverse firefighting conditions, respectively; and (3) clustered nodes confined to a local area.

Valve closure scheme varies with θ. Section 2.4 describes the potential influences of varying θ on flow availability. We examine the scheme across a range of θ values.

3. Illustrative Case Study

3.1. Overview of the Case

Figure 7a shows the ZJ network used to demonstrate the proposed approach. To ensure all nodes receive required water under normal operation, we adopted the network

modifications described in [18]. The network comprises 3 reservoirs, 116 demand nodes, and 166 pipelines, with P_{min} and P_{req} set to 0 and 20 m, respectively. All pipes are assumed to be located in non-liquefiable stiff alluvial soils and to be uniformly constructed of ductile iron.

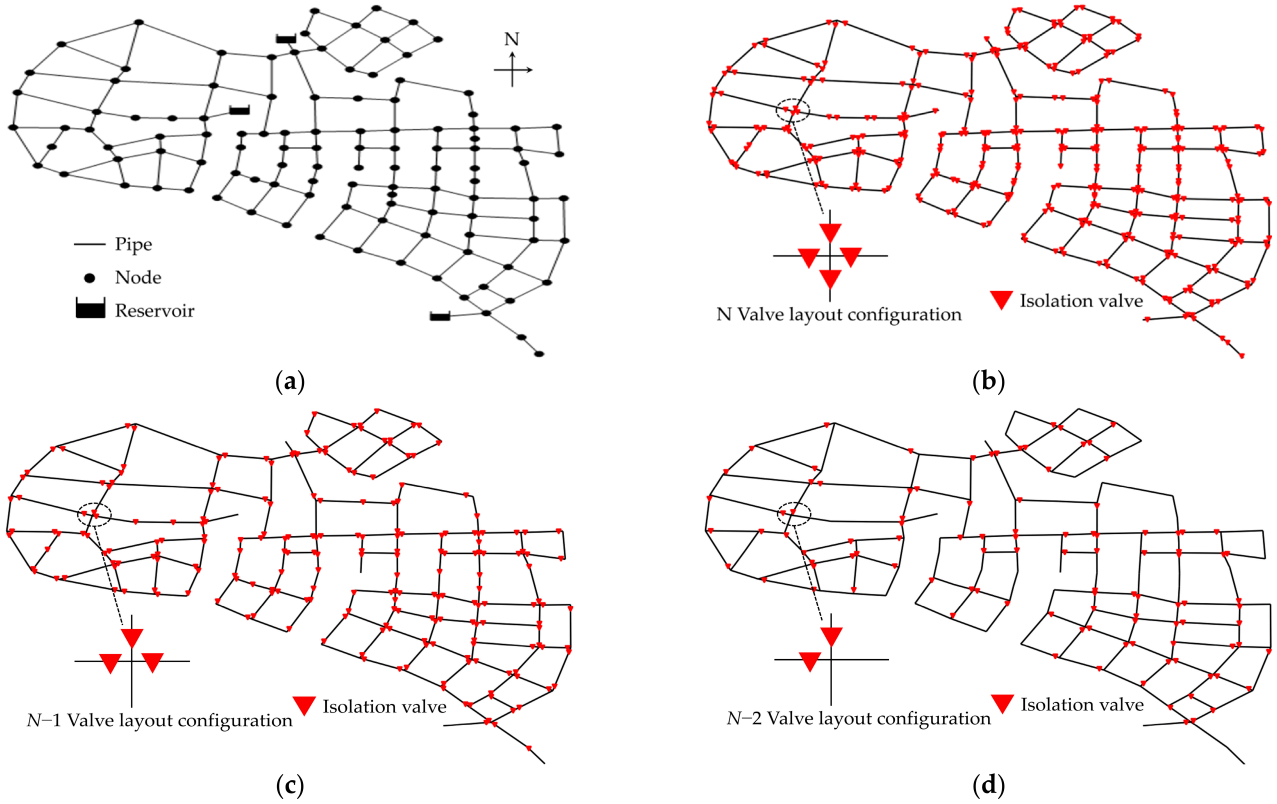


Figure 7. ZJ network and its valve-layout instances. (**a**) ZJ network. (**b**) N layout. (**c**) $N-1$ layout. (**d**) $N-2$ layout.

Firefighting parameters were set uniformly in accordance with Chinese national standards. Table 2 lists the design firefighting flow per fire as a function of population. Based on GB 5749-2022 [50], per capita water use is 0.12–0.20 m^3/d, implying a population of approximately 200,000–300,000 for this network; thus, $Q_i^{fire} = 0.06\ m^3/s$. According to GB 50137-2011 [51], per capita building floor area is 50 m^2, including 30–40 m^2 for residential use, 5.5 m^2 for commercial and public services, and 2 m^2 for transportation hubs. Accordingly, N_F is reported in Table 3. Pipe repair is generally not feasible within the selected time window and was therefore not considered. Following GB 50974-2014 [52], $P_{fire} = 10$ m.

Table 2. Design firefighting flow per fire event.

Population ($\times 10^4$)	≤1.0	1.0–2.5	2.5–5.0	5.0–10.0	10.0–20.0	20.0–30.0	30.0–40.0
Flow rate (m^3/s)	0.015	0.020	0.030	0.035	0.045	0.060	0.075

Table 3. Number of PEFs.

***pga* (*g*)**	0.11	0.12	0.13	0.14	0.15	0.16	0.17	0.18	0.19	0.20
N_F (N_{Fire})	2.1 (10.5)	2.3 (11.4)	2.5 (12.3)	2.6 (13.2)	2.8 (14.1)	3.0 (15.0)	3.2 (15.9)	3.4 (16.8)	3.5 (17.7)	3.7 (18.6)

3.2. Parameter Setup for Sensitivity Analysis

The parameters for sensitivity analysis were set as follows:

(1) Following [53], we considered earthquake scenarios with *pga* ranging from 0.10 to 0.20 *g*, and assumed spatially uniform ground motion intensity. We adopted a sample size of $N_S = 10000$, consistent with typical practice in analogous studies [6,11,13,19] and generally regarded as sufficient to capture scenario variability [7,54].

(2) Figure 7b–d show realizations of the N, $N-1$, and $N-2$ valve layouts. The N layout yields a single placement, while the $N-1$ and $N-2$ layouts allow multiple placements. Because a real WDN has only one valve placement, we used the instances in Figure 7c,d to compute assessment metrics. With the seismic damage–firefighting scenarios held constant, we replaced each valve instance with 50 randomly generated alternatives and used the resulting changes in the assessment metrics to examine whether valve placement influences firefighting capacity for a fixed layout.

(3) Table 3 shows that N_F ranges from 2 to 4. To examine firefighting capacity under more adverse conditions, we extended the upper limit to 6. Figure 8 displays the spatial distribution of satisfaction rates for *pga* = 0.17 *g* and serves to illustrate node selection. Fire nodes were chosen sequentially from the red nodes, then the blue nodes, and finally from all nodes to represent adverse, favorable, and random fire scenarios, respectively. To examine performance under spatially clustered fires, fire nodes were also selected inside the gray area. That area is supplied by both reservoirs R1 and R2 and therefore typically exhibits relatively favorable hydraulic conditions; examining it indicates how well-supplied regions respond to localized fire clusters.

(4) To assess how water curtailment and valve closure schemes affect firefighting capacity, we varied λ and θ over [0, 1] in 0.1 increments; these values represent curtailment severity from stringent to lenient and tolerance for increased hydraulic resistance from high to low, respectively. To assess the impact of required firefighting flow, we varied μ from 1.0 to 3.0 in 0.5 increments, representing required flow from the design value up to three times that value resulting from fire spread.

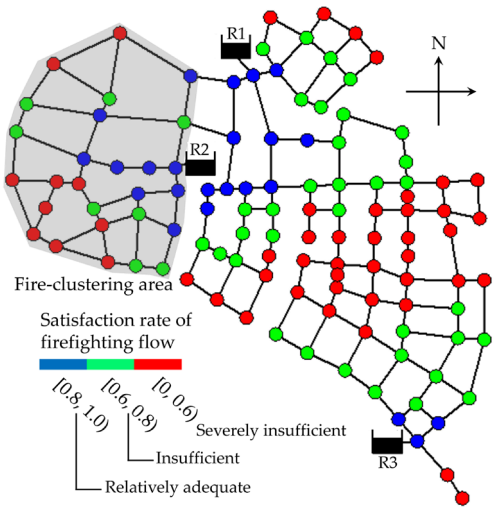


Figure 8. Spatial distribution of the firefighting flow satisfaction rate when *pga* = 0.17 *g*.

3.3. Results and Analysis

3.3.1. Effect of Valve Closure

Varying all factors simultaneously prevents isolating each factor's influence on firefighting capacity. Therefore, we first held λ, μ, and θ constant to examine how the remaining factors affect F_{fire} and then inferred the roles of these three factors from the resulting trends in F_{fire}. We fixed λ at 0.2 to represent a stringent domestic water limit that favors firefight-

ing flow, set μ to 1.0 to denote design flow needs, and fixed θ at 0.2 to indicate a strong propensity to isolate pipe breaks. Figure 9 shows how F_{fire} varies with *pga*, N_{F}, and fire spatial distribution for the no-valve case and for diverse valve layouts.

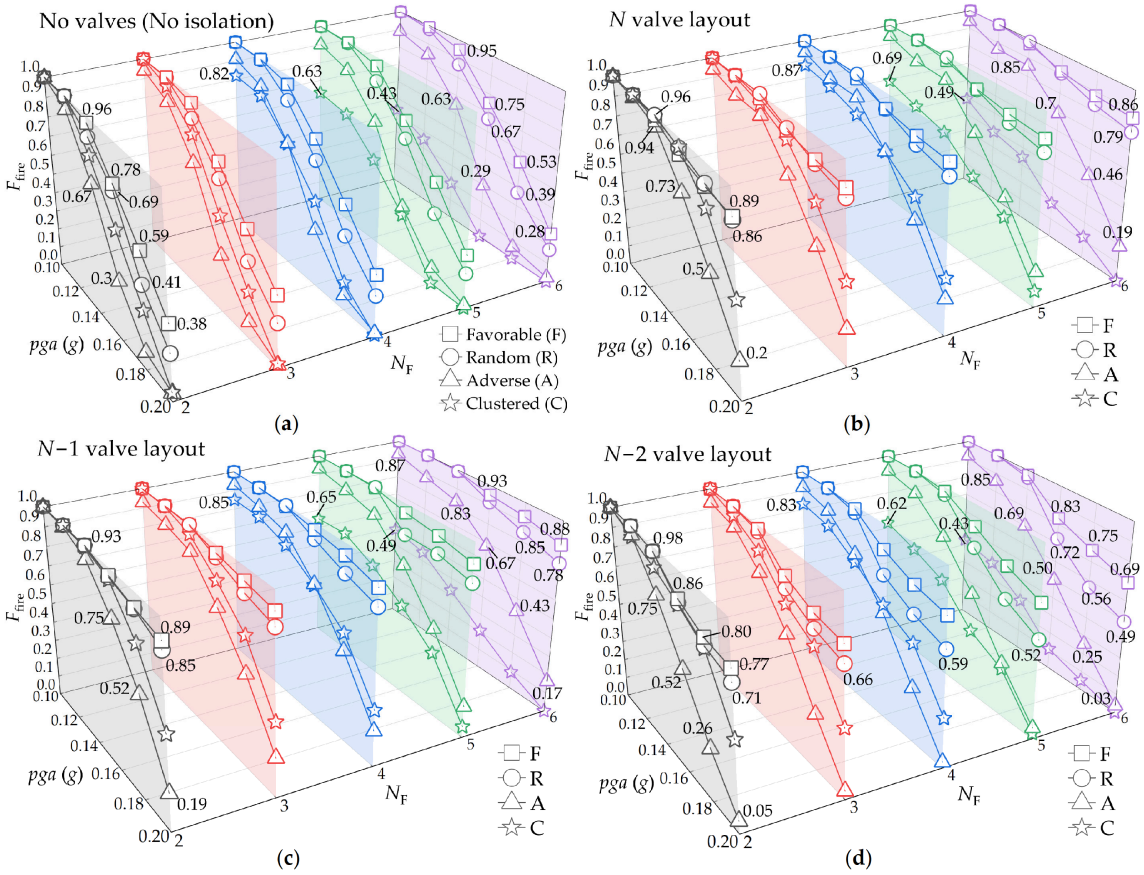


Figure 9. Variations in F_{fire} for no-valve case and for diverse valve layouts. (**a**) No valves. (**b**) N layout. (**c**) $N-1$ layout. (**d**) $N-2$ layout.

Comparison of Figure 9a–d shows that, without valves, F_{fire} declines more steeply as *pga* increases. Greater pipe damage at higher *pga* reduces the network's capacity to meet required firefighting flows, and the magnitude of this reduction depends on the spatial distribution of the fire. Under favorable scenarios, F_{fire} at $N_{\text{F}} = 2$ stays above 0.95 for $pga \leq 0.14\ g$ but falls to 0.59 at $pga = 0.18\ g$. Under adverse scenarios, F_{fire} at the same N_{F} drops below 0.7 at $pga = 0.14\ g$ and below 0.3 at $pga = 0.16\ g$. In these scenarios, F_{fire} changes little as N_{F} increases. However, under fire-clustering scenarios, F_{fire} falls from 1.0 to 0.43 even at $pga = 0.10\ g$. These results indicate that concentrated firefighting demand is potentially more hazardous because it is more likely to limit firefighting flow through hydraulic overloading than dispersed demand.

Figure 9b,c show that the N and $N-1$ layouts both improve firefighting capacity under favorable and random fire scenarios. F_{fire} remains above 0.8 even at $pga = 0.20\ g$ and is nearly identical for the N and $N-1$ layouts. By contrast, the $N-2$ layout produces a reduction in F_{fire}, falling from roughly 0.9 to 0.7 under favorable scenarios and from 0.8 to 0.5 under random scenarios. Under adverse and fire-clustering scenarios, however, even the N layout offers only limited benefit. In adverse scenarios, the system retains 73% of firefighting flow at $pga = 0.16\ g$ but only 20% at $pga = 0.20\ g$. In fire-clustering scenarios, the benefit of valve closure is weaker still: at $pga = 0.10\ g$, F_{fire} drops from 1.0 at $N_{\text{F}} = 2$ to 0.49 at $N_{\text{F}} = 6$, closely mirroring Figure 9a. These results indicate that, even under the most favorable N or $N-1$ layout, valve closure alone cannot restore flow losses when fires

occur in pressure-deficient or localized zones. Therefore, preventing these fire scenarios is preferable to relying solely on valve closure.

Figures 10 and 11 show F_{leak} and the number of isolated pipes with breaks, corroborating the improvement in firefighting in terms of leakage reduction. Figure 10a–c show that the N and $N-1$ layouts reduce leakage by 75% at pga = 0.12 and 0.16 g, and by 60% at pga = 0.20 g. Figure 11a shows that more than 90% of pipe breaks can be isolated. These results indicate that both layouts effectively curtail leakage and consequently yield comparable improvements in firefighting flow.

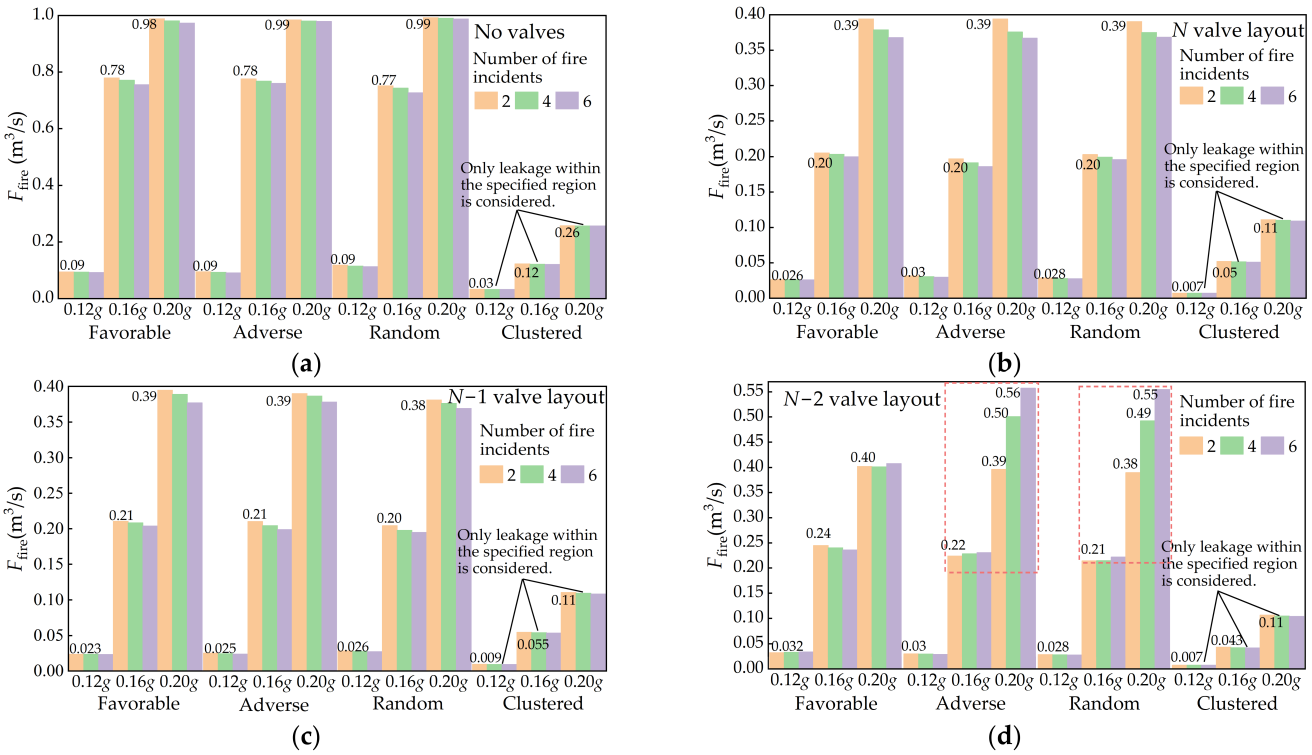


Figure 10. Variations in F_{leak} across different valve layouts. (**a**) No valves. (**b**) N layout. (**c**) $N-1$ layout. (**d**) $N-2$ layout.

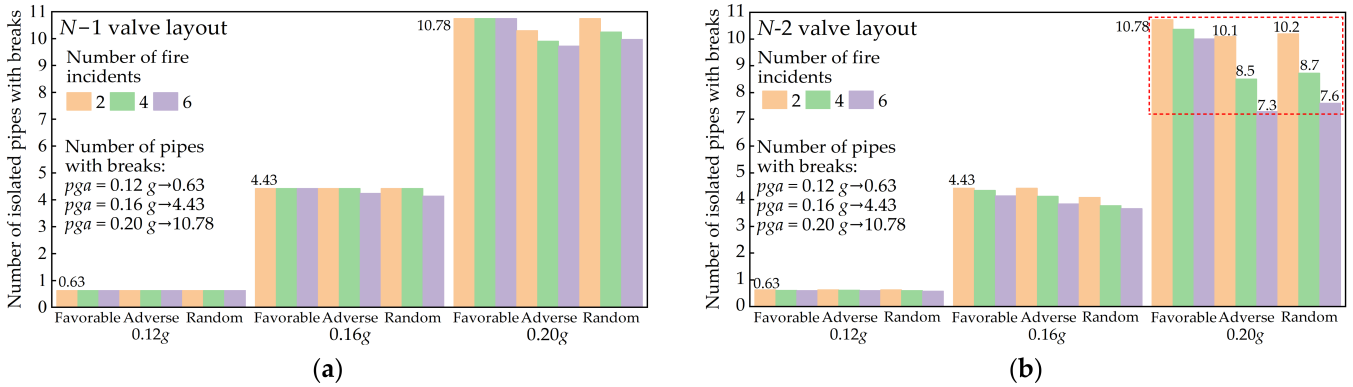


Figure 11. Number of isolated pipes with breaks. (**a**) $N-1$ layout. (**b**) $N-2$ layout.

By contrast, under the $N-2$ layout, the number of isolated breaks in Figure 11b decreases markedly with increasing pga and N_F. At pga = 0.20 g, as N_F increases from 2 to 6, isolated breaks in the adverse and random scenarios fall from 10.1 and 10.2 to 7.3 and 7.6, respectively, indicating that 10–30% of breaks remain open. The more sparse valves can produce larger isolated areas after valve closure. To preserve flow paths from sources to fire nodes, some breaks remain open, and this constraint becomes more pronounced as N_F

increases. As shown in Figure 10d, at pga = 0.20 g, leakage increases from roughly 0.2 to 0.55 with N_F in both adverse and random scenarios; this contributes to the less pronounced increase in F_{fire} observed in the corresponding cases in Figure 9d.

When fires cluster, flow concentration produces a steep pressure drop that primarily drives the reduction in F_{leak}. As shown in Figure 10, leakage in the specified zone is constrained, and therefore valve closure alone yields only limited recovery of firefighting flow, as shown in Figure 9.

Figure 12 shows the range of F_{fire} values for the 50 alternative valve placements under random and adverse scenarios. The placement of valves notably affects firefighting, particularly evident in the $N-2$ layout. In random scenarios (Figure 12a,b), $N-1$ placements sustain over 75% of the firefighting flow, while $N-2$ placements decrease F_{fire} from above 0.8 to 0.6 (pga = 0.20 g). The difference between the maximum and minimum F_{fire} values, denoted as $\Delta_{max-min}$, generally remains below 0.1 in the $N-1$ layout (Figure 12a,c) but can reach 0.2 in the $N-2$ layout (Figure 12b,d), leading to a decline of up to 20% in firefighting flow satisfaction. Given that the chosen placements are neither optimal nor worst-case scenarios, $\Delta_{max-min}$ could be larger. The $N-2$ layout can result in marked increases in pipe counts in certain segments due to improper placements, thereby expanding isolation and more markedly degrading water supply capacity. In contrast, the $N-1$ layout features a reduced number of pipes per segment, exhibiting minimal variation across different valve placements. Nevertheless, further optimizing valve placement could still improve firefighting flow satisfaction by approximately 10%.

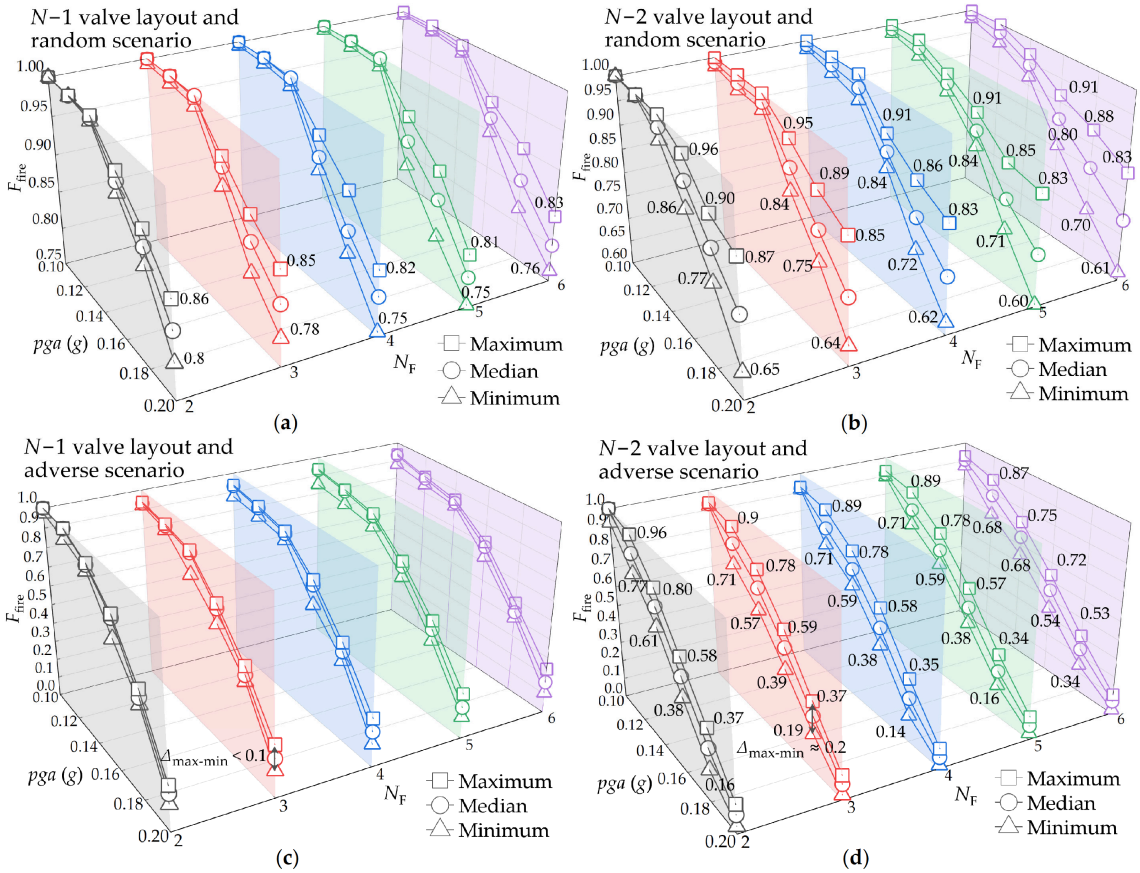


Figure 12. Variations in F_{fire} over the 50 alternative valve placements under the $N-1$ and $N-2$ layouts. (**a**) $N-1$ layout and random scenario. (**b**) $N-2$ layout and random scenario. (**c**) $N-1$ layout and adverse scenario. (**d**) $N-2$ layout and adverse scenario.

3.3.2. Effect of Required Domestic and Firefighting Flow

The preceding analysis indicates that, as *pga* increases, gains in F_{fire} under adverse and fire-clustering scenarios become negligible, even with the N layout. Thus, it is necessary to examine whether domestic water curtailment can reduce excess flow and thereby partially compensate for firefighting demand. Figure 13 shows the effect of λ on F_{fire} in these two scenarios, using representative values λ = 0.2, 0.5, 0.7, and 1.0.

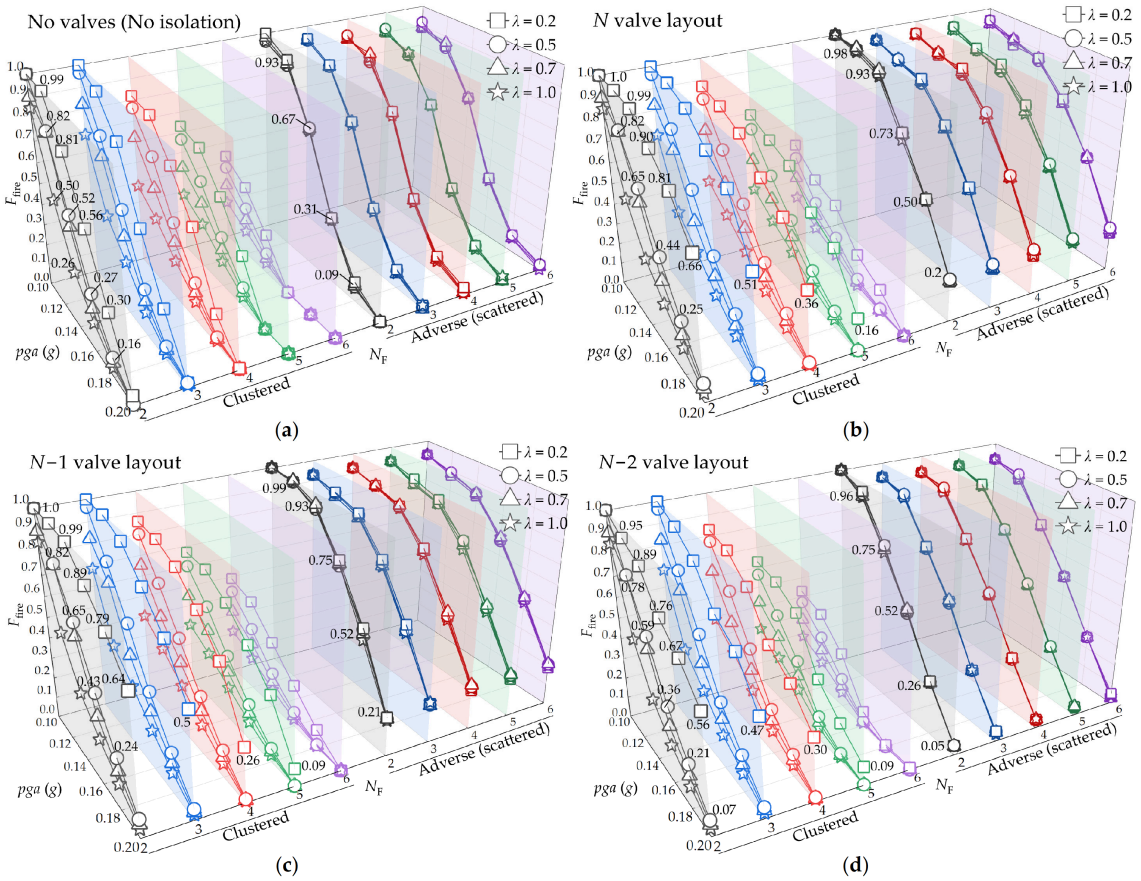


Figure 13. Variation in F_{fire} across representative values of λ under fire-clustering and adverse scenarios. (**a**) No valves. (**b**) N layout. (**c**) $N-1$ layout. (**d**) $N-2$ layout.

Under adverse scenarios, λ has little influence on F_{fire}; however, under fire-clustering scenarios, lowering λ improves F_{fire}. Under the no-valve case (Figure 13a), at $N_{\text{F}} = 2$ and pga = 0.14 g, λ = 0.2 preserves more than 80% of the firefighting flow, whereas λ = 0.5 or 0.7 maintains only 50%, and λ = 1.0 yields 26%. Figure 13b–d show that combining strict water curtailment with the N or $N-1$ layout provides effective improvement in firefighting flow, but only when N_{F} is small. For both layouts at $N_{\text{F}} = 2$, λ = 0.2 sustains 80% of firefighting flow for $pga \leq 0.18\ g$ and still achieves 66% at pga = 0.20 g. However, when λ = 0.5 and 0.7, F_{fire} decreases to zero as pga increases, at a rate comparable to the no-valve condition. Even at pga = 0.10 g, as N_{F} increases, λ = 0.2 cannot prevent a drop in F_{fire} from 1.0 to 0.4. Therefore, hydraulic overload resulting from concentrated firefighting flow may remain difficult to mitigate, even under strict domestic water curtailment and leakage control.

Figure 14 explains the variation in F_{fire} observed in Figure 13 by examining pressure recovery. Under fire-clustering scenarios, limited pipe damage at pga = 0.12 g keeps leakage low; consequently, valve layout has little effect on $\overline{P}_{\text{sys}}$ recovery (Figure 14a,c,e). In this regime, pressure loss is primarily driven by flow concentration, and higher N_{F} and λ further exacerbate the pressure decline. By contrast, severe damage at pga = 0.16 and 0.20 g makes leakage reduction a dominant contributor to pressure recovery. For the $N-1$ layout with

$N_F = 2$, $\overline{P}_{sys}$ recovers to 0.98 at pga = 0.16 g and remains 0.64 at pga = 0.20 g, indicating that the target area preserves relatively robust firefighting capacity. By contrast, relaxing λ to 0.5 reduces $\overline{P}_{sys}$ at pga = 0.16 g by 50% and drives it toward zero at pga = 0.20 g. Increasing N_F similarly produces a marked pressure decline. Pressure recovery under the $N-2$ layout is weaker than under $N-1$. Overall, the greatest pressure recovery is achieved when strict water curtailment is combined with the N or $N-1$ valve layout, but this benefit is evident only when N_F is small.

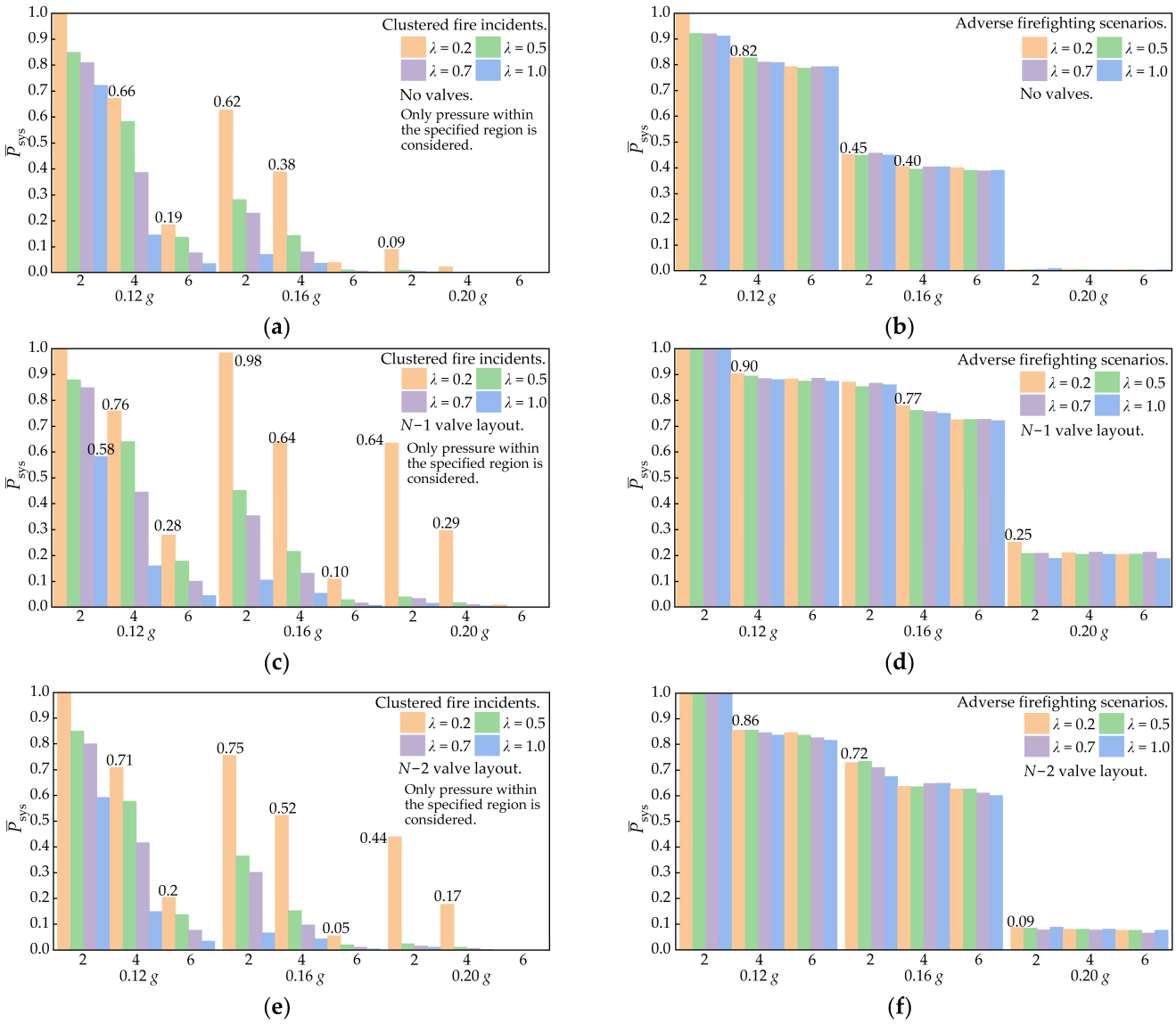


Figure 14. $\overline{P}_{sys}$ under fire-clustering and adverse scenarios. (**a**) No valves under fire-clustering scenarios. (**b**) No valves under adverse scenarios. (**c**) $N-1$ layout under fire-clustering scenarios. (**d**) $N-1$ layout under adverse scenarios. (**e**) $N-2$ layout under fire-clustering scenarios. (**f**) $N-2$ layout under adverse scenarios.

Under adverse scenarios, λ has little effect on $\overline{P}_{sys}$, whereas valve layout becomes the controlling factor. At pga = 0.16 g, the $N-1$ layout increases $\overline{P}_{sys}$ by approximately 100% relative to the no-valve case (Figure 14b,d), and the $N-2$ layout provides an improvement of 40–60% (Figure 14b,f). However, valve-layout benefits are limited by damage severity: at pga = 0.20 g, the $N-1$ layout restores pressure to only 25% of normal, and the $N-2$ layout restores it to only 10% of normal. This pattern matches the decline in F_{fire} with increasing

pga shown in Figures 9 and 13, indicating that even with the N valve layout, a severely degraded hydraulic state can prevent adequate firefighting flow from being maintained.

Figure 15 shows the relationship between F_{fire} and μ under λ = 0.2 and random scenarios to investigate if the escalation of required firefighting flow leads to hydraulic overload more than λ and N_{F}. F_{fire} notably decreases with increasing μ, a trend accentuated by higher N_{F}. In the $N-1$ layout with $N_{\text{F}} = 2$, $\mu = 3.0$ decreases F_{fire} by over 10% at *pga* = 0.14 *g* and by 16% at *pga* = 0.20 *g* compared to the design flow ($\mu = 1.0$); with $N_{\text{F}} = 6$, the reduction extends to 20% at *pga* = 0.20 *g*. Under the $N-2$ layout, for *pga* $\geq$ 0.14 *g*, $\mu = 3.0$ lowers F_{fire} by roughly 15–25% relative to the design condition. With an increase in N_{F}, combined firefighting flows markedly intensifies head loss from sources to fire nodes and thus exacerbate pressure decline at fire nodes. Consequently, a sharp rise in required firefighting flow at a few fire nodes can induce more severe hydraulic overload than numerous fire nodes, each with only the design flow.

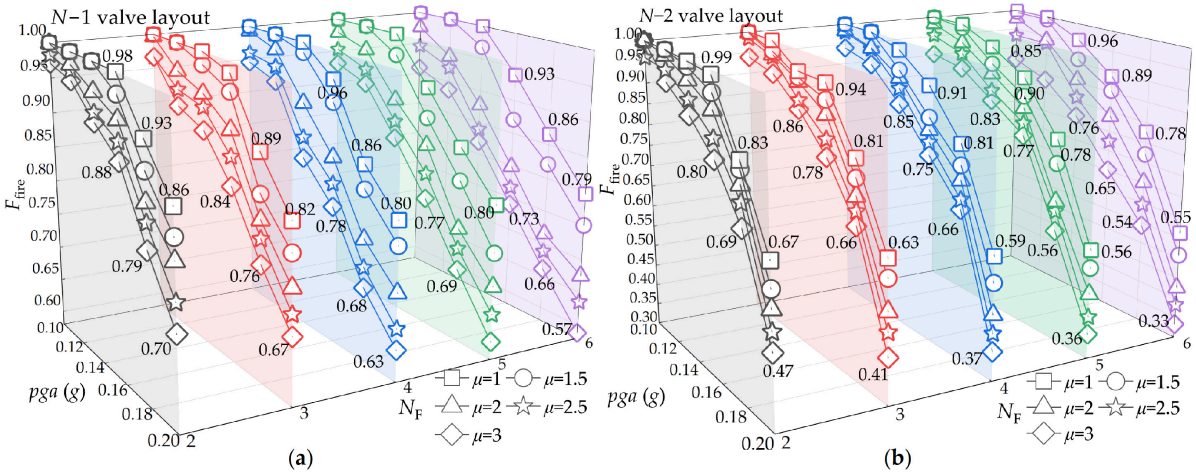


Figure 15. Variations in F_{fire} across representative values of μ under random scenarios. (**a**) $N-1$ layout. (**b**) $N-2$ layout.

3.3.3. Effect of Valve Closure Scheme

Figure 16 shows how the aggressiveness of valve closure can enhance improvements in firefighting flow by illustrating the effect of θ on F_{fire}, with representative values of θ = 0.2, 0.6, and 1.0. θ = 1.0 necessitates that the highest-capacity transmission paths from sources to fire nodes remain entirely connected. Consequently, under this condition, F_{fire} serves as a baseline derived from the original method [38]. To investigate the efficacy of isolation, we contrast these outcomes against three scenarios: no isolation, optimal isolation, and complete isolation. We enumerate all isolation schemes and compute the corresponding F_{fire} for each. The scheme that maximizes F_{fire} is defined as the optimal isolation. Complete isolation entails isolating all pipe breaks, aligning with the isolation of localized breaks [34,35]. Owing to the minimal difference between the N and $N-1$ layouts, we present results exclusively for $N-1$ and $N-2$.

The result indicates that the relaxation mechanism can enhance firefighting flow satisfaction compared to the original method. In both the $N-1$ and $N-2$ layouts, the values of F_{fire} at θ = 0.2 and θ = 0.6 are approximately equal and both exceed the value at θ = 1.0. The disparity between θ = 0.2 and θ = 1.0 is most pronounced for *pga* = 0.14–0.18 *g*: F_{fire} at θ = 0.2 surpasses that at θ = 1.0 by roughly 0.1 under the $N-1$ layout and by 0.05–0.1 under the $N-2$ layout. Compared with the condition of no isolation, the scheme at θ = 0.2 markedly enhances firefighting flow for *pga* = 0.14–0.18 *g*, increasing F_{fire} by 0.3–0.5 under the $N-1$ layout and by 0.1–0.2 under the $N-2$ layout. However, this scheme remains 0.05–0.1 below optimal isolation, indicating

that the proposed method offers effective solutions but does not achieve the optimum. Complete isolation improves F_{fire} only for $pga \leq 0.12\ g$; under the $N-2$ layout, it is even less effective than no isolation. To elucidate these differences, Table 4 compares the proposed method with optimal and complete isolation regarding leakage, pressure, and average firefighting flow availability.

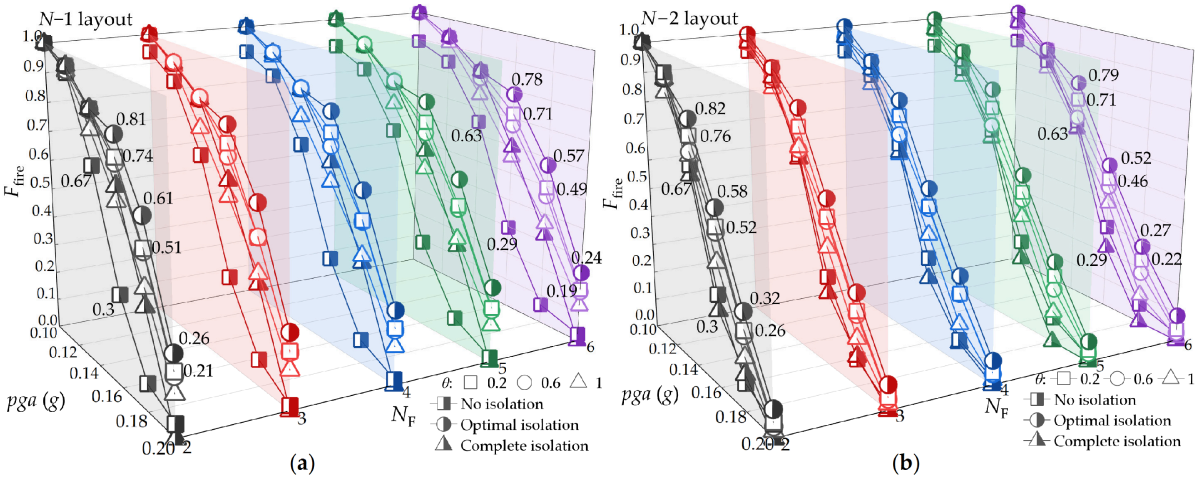


Figure 16. Variation in F_{fire} across representative values of θ under adverse scenarios. (**a**) $N-1$ layout. (**b**) $N-2$ layout.

Table 4. Leakage, pressure, and flow availability metrics under diverse valve closure schemes.

pga (*g*)	Valve Layout	Valve Closure Scheme	F_{leak}		$\bar{P}_{\text{sys}}$		f	
			$N_F = 3$	$N_F = 6$	$N_F = 3$	$N_F = 6$	$N_F = 3$	$N_F = 6$
0.12	$N-1$	This method ($\theta = 0.2$)	0.025	0.025	0.91	0.90	1	1
		Optimal isolation	0.025	0.025	0.91	0.90	1	1
		Complete isolation	0.025	0.025	0.90	0.90	1	0.99
	$N-2$	This method ($\theta = 0.2$)	0.03	0.03	0.86	0.83	0.98	0.98
		Optimal isolation	0.03	0.03	0.89	0.89	0.92	0.92
		Complete isolation	0.028	0.023	0.79	0.78	0.86	0.87
0.16	$N-1$	This method ($\theta = 0.2$)	0.20	0.18	0.82	0.75	0.79	0.79
		Optimal isolation	0.18	0.15	0.90	0.82	0.67	0.66
		Complete isolation	0.12	0.10	0.68	0.62	0.46	0.46
	$N-2$	This method ($\theta = 0.2$)	0.23	0.24	0.71	0.60	0.70	0.70
		Optimal isolation	0.16	0.17	0.80	0.66	0.55	0.55
		Complete isolation	0.08	0.08	0.34	0.28	0.23	0.23
0.20	$N-1$	This method ($\theta = 0.2$)	0.39	0.37	0.23	0.20	0.66	0.66
		Optimal isolation	0.31	0.31	0.31	0.27	0.57	0.56
		Complete isolation	0.02	0.04	0.06	0.01	0.29	0.29
	$N-2$	This method ($\theta = 0.2$)	0.40	0.56	0.09	0.08	0.59	0.58
		Optimal isolation	0.32	0.42	0.16	0.15	0.44	0.45
		Complete isolation	0.15	0.15	≈0	≈0	≈0	≈0

First, at $\theta = 0.2$, f of the proposed method decreases as *pga* increases, then stabilizes near 0.6–0.7 at $pga = 0.20\ g$. Because f stays within this range, $\theta = 0.2$ and $\theta = 0.6$ produce similar outcomes: both preserve paths' transmission capacity while adequately isolating pipe breaks, thereby improving firefighting flow. In comparison, full connectivity of high-capacity paths (at $\theta = 1.0$) prevents many pipe breaks from being isolated, thereby weakening leakage mitigation.

Second, except for pga = 0.12 g under the $N-1$ layout, optimal isolation generally produces f values 0.1–0.15 lower than the proposed method, while producing 0.05–0.1 higher residual pressure and leakage reduction. Because the looped network provides many alternative paths between sources and fire nodes, estimating capacity based only on independently high-capacity paths underestimates the network's transmission capability. This underestimation results in the gap between the proposed scheme and the optimal one.

Third, at pga = 0.12 g, pipe breaks are sparse, and complete isolation yields F_{leak}, $\overline{P}_{\text{sys}}$, and f values similar to the other two methods. At pga = 0.16 or 0.20 g, complete isolation minimizes F_{leak} and thus produces the strongest leakage control, but both f and $\overline{P}_{\text{sys}}$ decline sharply. This pattern indicates that high-capacity paths from sources to fire nodes are severed and many nodes become isolated from the network. This effect is most pronounced under the $N-2$ layout: at pga = 0.16 g, the pressure is only half that of the proposed method, and at pga = 0.20 g, it is nearly zero. In this layout, each segment contains more pipes, so isolating additional pipes more severely degrades transmission capacity, underscoring the need for a rational valve closure decision method.

To quantify the relative difference between the proposed method and optimal isolation, we define Δ as the normalized difference between their F_{fire} values, using the optimal value as the denominator. Table 5 reports the percentage of scenarios in which Δ falls within each interval. Smaller Δ values indicate closer agreement with the optimum, with $\Delta = 0$ denoting identical schemes. Thus, a larger share of scenarios with small Δ signifies that the method more robustly yields near-optimal isolation schemes.

Table 5. Percentage of scenarios with Δ within each given range.

pga (g)	Valve Layout	N_F	Percentage of Scenarios (%)			
			$\Delta > 0.2$	$0.1 < \Delta \leq 0.2$	$0 < \Delta < 0.1$	$\Delta = 0$
0.12	$N-1$	3	0	≈0	4	96
		6	0	≈0	6	94
	$N-2$	3	0	≈0	4	96
		6	2	≈0	8	92
0.16	$N-1$	3	4	34	39	23
		6	7	34	35	24
	$N-2$	3	13	35	30	22
		6	16	35	28	21
0.20	$N-1$	3	19	43	26	12
		6	21	44	25	10
	$N-2$	3	32	38	22	8
		6	36	37	21	5

The results show that the robustness of yielding near-optimal isolation schemes relies on ground motion intensity and valve layout. At pga = 0.12 g, network damage is minimal, $\Delta = 0$ predominates, and $\Delta > 0.1$ is rare, which indicates the method almost always yields schemes identical or very close to the optimum. At pga = 0.16 g, the fraction of low Δ values fall substantially: the proportion of scenarios in which the proposed scheme matches the optimal one falls below 25%, while 40–50% of scenarios exhibit $\Delta > 0.1$. Notably, under the $N-2$ layout, about 16% of scenarios have $\Delta > 0.2$. At pga = 0.20 g, Δ increases further: over 60% of scenarios have $\Delta > 0.1$. Furthermore, under the $N-2$ layout, 36% of scenarios have $\Delta > 0.2$, indicating a widening gap between the proposed method's scheme and the optimum. As pga increases, an increasing number of small leaks along high-capacity transmission paths collectively produce substantial loss and degrade effective capacity. Hence, the proposed method may misidentify which path can deliver the most water.

Isolating pipe breaks under sparser valve layouts enlarges the isolation area and markedly reduces the number of water-transmission paths, which makes the network sensitive to the choice of isolated pipes. The proposed scheme does not fully account for these hydraulic changes, so it is more likely to deviate from the optimal solution. Consequently, refining the valve closure scheme with hydraulics-based heuristics is required to close this gap.

4. Discussion

4.1. Methodological Contributions to Prior Studies

We integrate an improved valve closure decision method into post-earthquake firefighting capacity assessment [6,18] and uses a case study to delineate the conditions under which valve closure enhances firefighting capacity. The effectiveness of isolating breaks to bolster firefighting capacity is constrained by multiple factors.

(1) Valve layout and placement strongly influence firefighting flow. The $N-1$ layout outperforms $N-2$ in mitigating resulting impacts of isolation. Valve placement can exert a non-negligible influence for the $N-2$ layout. Therefore, when the number of valves is limited, their locations should be planned deliberately to maximize firefighting capacity.

(2) Severe seismic damage can produce extensive pipe leaks that valve closure cannot control, preventing restoration of firefighting flow. This observation aligns with [18] and indicates that seismic retrofit is effective for bolstering firefighting capacity.

(3) As reported in [6,18], fires in pressure-deficient areas are more likely to become uncontrollable, particularly when the network sustains severe damage; in such cases, valve closure may not effectively mitigate the risk. Extending the focus of [6] to domestic water use, clustered fires can amplify the vulnerability of firefighting flow to rising domestic water and to increases in fire count; therefore, such scenarios should be avoided.

(4) Valve closure cannot sustain the stable flow required at fire nodes when demand surges. Building on [6], a sharp increase in required flow at a few nodes can produce more severe consequences than an equivalent design flow demand distributed across multiple fires, particularly under the $N-2$ layout.

(5) Incorporating a mechanism that balances leakage reduction with water-transmission capacity into the valve closure decision method proposed in [38] can further improve firefighting flow. However, the transmission capacity estimated from hydraulic resistance still deviates from actual flow, yielding an average discrepancy of 5–10% in the flow satisfaction rate. The method should be tested on additional networks to assess its generality. The sensitivity analysis can be used to narrow a plausible θ range, and the optimal θ can be identified by combining that range with operational data and engineering judgment.

Although these findings are case-specific, the analytical framework can be applied to other networks to broaden understanding of how multiple factors shape the role of valve closure in firefighting capacity.

4.2. Methodological Contributions to SDGs

Beyond the contributions summarized in Section 4.1, the method supports sustainable, resilient infrastructure management by enabling condition-specific valve closure decisions that balance leakage control with firefighting supply. It also guides the allocation of retrofit and emergency resources to enhance a WDN's firefighting capacity.

These contributions support SDGs 9 and 11. For SDG 9, this study advances Target 9.1 on resilient infrastructure and Target 9.5 on research and technological capacity by improving the seismic-resilience analysis of WDNs. For SDG 11, it advances Target 11.5 on

reducing disaster losses and Target 11.b on disaster-risk management by providing an actionable decision-support tool. It also facilitates allocation of retrofit and emergency resources, thereby supporting Target 11.1 on safe and affordable basic services.

4.3. Limitations and Future Directions

(1) Seismic damage modeling. To prevent multiple failure modes from obscuring the effect of valve closure decisions on firefighting capacity, we employed simplified damage scenarios, which may overestimate the benefits of valve closure. For example, valve failures would prevent planned closures, damage to pumps or power systems would limit achievable firefighting flow, permanent ground deformation and liquefaction can yield far more extensive pipe breaks, and independent and homogeneous damage conditions can underestimate spatially clustered pipe damage. Future work should incorporate valve failures into seismic damage models and develop scenarios that account for spatially correlated ground motion, site conditions, and multi-component failures to more realistically assess the limits of valve closure for enhancing firefighting capacity.

(2) Fire scenario modeling. We generated fire scenarios without accounting for spatial heterogeneity, so the simulated spatial distribution of fires may differ from that of real events. If real fires tend to cluster in low-pressure areas, the risk of uncontrolled fires could exceed the estimates reported here. Similarly, assuming static ignitions ignores temporal variations in required firefighting flow. Future research should develop fire-spread models informed by environmental data [55] and couple them with hydraulic models to compare available and required flow dynamically.

(3) Water rationing planning. This study does not account for essential demands (e.g., medical rescue and critical energy production) during post-earthquake response. Future work should develop water-rationing plans that incorporate user priorities, demand elasticity, and temporal usage patterns. While ensuring the required firefighting flow, differentiated rationing plans by time and user are needed to mitigate the impacts of flow shortages on residential and critical services.

(4) Valve closure decision method. We conducted the analysis on a computer with an AMD 9575F @ 3.3 GHz CPU and 384 GB of RAM; generating a valve closure decision for each scenario took on average less than 5 s. The shortest-path algorithm imposes minimal computational cost, but enumeration of all valve closure schemes remains wasteful. Thus, before integrating hydraulic simulation into the decision method to increase robustness, enumeration should be replaced with heuristic methods to balance decision accuracy and computational efficiency. The method must also be tested on WDNs with varied topologies and, for any fixed valve layout, across alternative valve placements to clarify the conditions under which valve closure effectively improves firefighting capacity.

5. Conclusions

This study develops an improved valve closure decision method for WDNs under post-earthquake firefighting conditions, aiming to reduce leakage while limiting impacts on water transmission capacity. Applied to a benchmark network, we examine how factors related to pipe damage, fire scenarios, required flow, valve layout, and closure policy jointly influence the effectiveness of valve closure in enhancing firefighting. The principal findings are as follows:

(1) In the case study, the improved method increases firefighting flow satisfaction but still falls short of optimal isolation by an average of 5–10%. This deficit arises because estimates for high-capacity paths underestimate actual water transmission capacity,

causing the method to discard some near-optimal schemes. When seismic damage and fires are limited under the $N-1$ valve layout, the method frequently produces near-optimal isolation schemes and matches the optimal solution in over 90% of scenarios. By contrast, when damage and fires are numerous under the $N-2$ layout, the method's robustness in producing near-optimal isolation schemes declines.

(2) The case study indicates that isolating pipe breaks improves firefighting capacity when it recovers pressure at fire nodes. This outcome is most likely when pipe damage is limited, fires are few, and fire nodes are scattered in areas with adequate pressure. Curtailing domestic water helps only if it compensates for the extra head loss caused by firefighting flow and leakage. Strategic valve placement reduces the impact on firefighting by decreasing the isolated area. Valve closure alone is insufficient in several situations: widespread pipe leaks resulting from strong ground motion; clustered fires or large surges in firefighting flow that induce hydraulic overload; fire nodes in zones where pressure falls sharply owing to excessive flow or leakage; and sparse valve layouts in which poor valve placement greatly enlarges the isolation area. In these cases, complementary measures are required, including seismic retrofitting of pipes, removal of fire hazards, and, above all, prevention of simultaneous fires in low-pressure or localized zones.

These findings are limited to the benchmark network and to simplified assumptions (e.g., independent pipe damage, fully operational valves and water sources). Future work should refine the decision method with hydraulics-based heuristics, investigate networks of varying sizes and configurations under alternative valve placements, and apply realistic scenarios of seismic damage to improve the realism and generalizability of the results.

Supplementary Materials: The following supporting information can be downloaded at: https://www.mdpi.com/article/10.3390/su182110882/s1. The convergence of the Monte Carlo estimates is examined in Section S1 of the Supplementary Materials. Figure S1: Relative deviation of F_{fire}, F_{leak}, or $\overline{P}_{\text{sys}}$ across representative sample sizes; Section S2: Benchmark-network data (in EPANET .inp format).

Author Contributions: Conceptualization and Methodology, X.H. and C.Z.; Writing—original draft, X.H.; Writing—review and editing, H.H.; Supervision, H.H. and T.Q.; Funding acquisition, C.Z. and T.Q. All authors have read and agreed to the published version of the manuscript.

Funding: This research was funded by the Central Public-Interest Scientific Institution Basal Research Fund (Grant No. 512025Y-12520) and the National Natural Science Foundation of China (Grant No. 72274181).

Institutional Review Board Statement: Not applicable.

Informed Consent Statement: Not applicable.

Data Availability Statement: The original benchmark-network data were obtained from the database: http://www.uky.edu/WDST/database.html (accessed on 17 July 2026). The modified network input data have been submitted as Supplementary Materials. Parameter sets, randomization procedures, and valve-closure decision method are provided in sufficient detail. The computational code is available from the corresponding authors upon reasonable request.

Acknowledgments: The authors appreciate the reviewers for their help in highlighting deficiencies in this study.

Conflicts of Interest: The authors declare no conflicts of interest, and the funders had no role in the process of this study.

References

1. Ayik, U.; Tagil, S.; Ögel, C.; Sen, Ö.; Bilim, Z.O.; Tunç, T.B.; Durmus, B.S.; Ayik, Z.; Demir, S.; Isibol, I. Mixed-methods analysis of post-earthquake displacement and residential mobility after the 2020 Aegean Sea Earthquake: Implications for urban sustainability in İzmir. *Sustainability* **2026**, *18*, 5607. [CrossRef]
2. Coar, M.; Sarreshtehdari, A.; Garlock, M.; Khorasani, N.E. Methodology and challenges of fire following earthquake analysis: An urban community study considering water and transportation networks. *Nat. Hazards* **2021**, *109*, 1–31. [CrossRef]
3. Scawthorn, C.; O'Rourke, T.D.; Blackburn, F.T. The 1906 San Francisco earthquake and fire—Enduring lessons for fire protection and water supply. *Earthq. Spectra* **2006**, *22*, 135–158. [CrossRef]
4. Behnam, B. *Post-Earthquake Fire Analysis in Urban Structures: Risk Management Strategies*, 1st ed.; CRC Press Taylor & Francis Group: Boca Raton, FL, USA, 2016. [CrossRef]
5. Lou, T.; Wang, W.; Izzuddin, B.A. A framework for performance-based assessment in post-earthquake fire: Methodology and case study. *Eng. Struct.* **2023**, *294*, 116766. [CrossRef]
6. Hou, G.J.; Li, Q.W. Firefighting capacity evaluation of water distribution system subjected to multi-ignitions of post-earthquake fires. *Struct. Saf.* **2021**, *88*, 102035. [CrossRef]
7. Hou, B.W.; Xu, Q.Y.; Zhong, Z.L.; Han, J.Y.; Miao, H.Q.; Du, X.L. Seismic reliability evaluation of spatially correlated pipeline networks by quasi-Monte Carlo simulation. *Struct. Infrastruct. Eng.* **2024**, *20*, 498–513. [CrossRef]
8. Federal Emergency Management Agency (FEMA). *HAZUS97 Technical Manual*; FEMA: Washington, DC, USA, 1997.
9. American Lifelines Alliance. *Seismic Fragility Formulations for Water Systems Part 1 Guideline*; American Lifeline Alliance: Washington, DC, USA, 2001.
10. Long, L.; Yang, H.P.; Zheng, S.S.; Cai, Y.L. Seismic resilience evaluation of urban multi-age water distribution systems considering soil corrosive environments. *Sustainability* **2024**, *16*, 5126. [CrossRef]
11. Jia, R.; Du, K.; Song, Z.G.; Xu, W.; Zheng, F.F. Scenario reduction-based simulation method for efficient serviceability assessment of earthquake-damaged water distribution systems. *Reliab. Eng. Syst. Saf.* **2024**, *246*, 110086. [CrossRef]
12. Hou, B.W.; Yang, C.X.; Wu, S.; Miao, H.Q.; Xu, C.S. Seismic retrofit optimization of water distribution systems based on the reduction of uncertain damage scenarios. *Int. J. Disast. Risk Reduct.* **2024**, *112*, 104756. [CrossRef]
13. GIRAFFE. *GIRAFFE User's Manual*; School of Civil and Environmental Engineering, Cornell University: Ithaca, NY, USA, 2008.
14. Yoo, D.G.; Jung, D.; Kang, D.; Kim, J.H.; Lansey, K. Seismic hazard assessment model for urban water supply networks. *J. Water Resour. Plan. Manag.* **2016**, *142*, 04015055. [CrossRef]
15. Klise, K.A.; Bynum, M.; Moriarty, D.; Murray, R. A software framework for assessing the resilience of drinking water systems to disasters with an example earthquake case study. *Environ. Model. Softw.* **2017**, *95*, 420–431. [CrossRef] [PubMed]
16. Kanta, L.; Brumbelow, K. Vulnerability, risk, and mitigation assessment of water distribution systems for insufficient fire flows. *J. Water Resour. Plan. Manag.* **2013**, *139*, 593–603. [CrossRef]
17. Kanta, L.; Zechman, E.; Brumbelow, K. Multiobjective evolutionary computation approach for redesigning water distribution systems to provide fire flows. *J. Water Resour. Plan. Manag.* **2012**, *138*, 144–152. [CrossRef]
18. Li, W.N.; Mazumder, R.K.; Bastidas-Arteaga, E.; Li, Y. Seismic performance evaluation of corroded water distribution systems considering firefighting. *J. Water Resour. Plan. Manag.* **2024**, *150*, 04023075. [CrossRef]
19. Li, Y.Z.; Gao, J.L.; Zhang, H.Y.; Deng, L.Q.; Xin, P. Reliability assessment model of water distribution networks against fire following earthquake (FFE). *Water* **2019**, *11*, 2536. [CrossRef]
20. Chu-Ketterer, L.J.; Murray, R.; Hassett, P.; Kogan, J.; Klise, K.; Haxton, T. Performance and resilience analysis of a New York drinking water system to localized and system-wide emergencies. *J. Water Resour. Plan. Manag.* **2023**, *149*, 05022015. [CrossRef] [PubMed]
21. Liu, X.L.; Zhang, M.Y.; Liu, H.X. Resilience-based multi-objective optimization of failure response strategies in water distribution systems. *Reliab. Eng. Syst. Saf.* **2026**, *267*, 111883. [CrossRef]
22. Zhang, J.; Li, Y.; Yuan, H.Q.; Du, G.F.; Zhang, M.Y. A demand-based three-stage seismic resilience assessment and multi-objective optimization method of community water distribution networks. *Reliab. Eng. Syst. Saf.* **2024**, *250*, 110279. [CrossRef]
23. Zheng, Z.X.; Zheng, F.F.; Qi, Z.X.; Wen, J.H.; Chen, J.Y.; Duan, H.F.; Savic, D.; Kapelan, Z. Improving the understanding of secondary impacts of isolation valve closures on the performance of water distribution systems. *J. Water Resour. Plan. Manag.* **2024**, *150*, 04024023. [CrossRef]
24. Liu, H.; Walski, T.; Fu, G.; Zhang, C. Failure impact analysis of isolation valves in a water distribution network. *J. Water Resour. Plan. Manag.* **2017**, *143*, 04017019. [CrossRef]
25. Beker, B.A.; Kansal, M.L. Pipe and isolation valve failure-impact analysis and prioritization model for an urban water distribution network. *J. Hydroinform.* **2023**, *25*, 491–510. [CrossRef]
26. Giustolisi, O.; Berardi, L.; Laucelli, D. Optimal water distribution network design accounting for valve shutdowns. *J. Water Resour. Plan. Manag.* **2014**, *140*, 277–287. [CrossRef]

27. Liu, J.; Wan, Y.; Zhang, Q.; Wang, H.; Zhao, D.; Wei, D.; Zhu, Y.; Liu, J. Optimization of isolation valve placement to improve reliability and resilience of water distribution systems. *Reliab. Eng. Syst. Saf.* **2024**, *252*, 110423. [CrossRef]
28. Abhijith, G.R.; Salomons, E.; Ostfeld, A. Developing a simplified practical approach for analyzing the criticality of isolation valves. *J. Water Resour. Plan. Manag.* **2023**, *149*, 06023005. [CrossRef]
29. Jiao, H.M.; Hu, Z.; Yang, Z.J.; Zeng, W.; Xu, F.; Han, C.Y. Hierarchical structure-based model for importance and reliability assessment of water distribution networks. *Reliab. Eng. Syst. Saf.* **2025**, *253*, 110542. [CrossRef]
30. Liu, X.L.; Zhang, M.Y.; Liu, H.X. Optimization of isolation valve operation and identification of critical components for enhancing the resilience of water distribution systems. *Reliab. Eng. Syst. Saf.* **2026**, *273*, 112387. [CrossRef]
31. Trapiello, C.; Romero-Ben, L.; Meseguer, J.; Puig, V.; Cembrano, G.; Joseph-Duran, B.; Sarrias, M.; Saporta, D.; Minoves, M. Automatic network response methodology for failure recovery or bursts in drinking water networks. *J. Water Resour. Plan. Manag.* **2023**, *149*, 04022073. [CrossRef]
32. Nikoloudi, E.; Romano, M.; Memon, F.A.; Kapelan, Z. Heuristic-based approach for near-optimal response to water distribution network failures in near real time. *J. Water Resour. Plan. Manag.* **2022**, *148*, 04022039. [CrossRef]
33. Nerantzis, D.; Stoianov, I. Adaptive model predictive control for fire incidents in water distribution networks. *J. Water Resour. Plan. Manag.* **2022**, *148*, 04021102. [CrossRef]
34. Hernandez, E.H.; Ormsbee, L. Segment-based assessment of consequences of failure on water distribution systems. *J. Water Resour. Plan. Manag.* **2021**, *147*, 04021009. [CrossRef]
35. Alvisi, S.; Franchini, M. A heuristic procedure for the automatic creation of district metered areas in water distribution systems. *Urban Water J.* **2014**, *11*, 137–159. [CrossRef]
36. Choi, J.; Kang, D. Improved Hydraulic Simulation of valve layout effects on post-earthquake restoration of a water distribution network. *Sustainability* **2020**, *12*, 3492. [CrossRef]
37. Zhang, Q.Z.; Zheng, F.F.; Chen, Q.W.; Kapelan, Z.; Diao, K.G.; Zhang, K.J.; Huang, Y. Improving the resilience of postdisaster water distribution systems using dynamic optimization framework. *J. Water Resour. Plan. Manag.* **2020**, *146*, 04019075. [CrossRef]
38. Li, Y.Z.; Gao, J.L.; Jian, C.; Ou, C.H.; Hu, S.Y. A Two-Stage Post-Disaster Response and Restoration Method for the Water Distribution System. In Proceedings of the 1st International WDSA/CCWI Joint Conference, Kingston, ON, Canada, 23–25 July 2018. No. 117.
39. Klise, K.A.; Hart, D.B.; Bynum, M.; Hogge, J.; Haxton, T.; Murray, R.; Burkhardt, J. *Water Network Tool for Resilience (WNTR) User Manual: Version 1.0*; EPA/600/B-23/098; U.S. EPA Office of Research and Development: Washington, DC, USA, 2023.
40. Rossman, L.A.; Woo, H.; Tryby, M.; Shang, F.; Janke, R.; Haxton, T. *EPANET 2.2 User Manual*; EPA/600/R-20/133; U.S. Environmental Protection Agency: Washington, DC, USA, 2020.
41. Wagner, J.M.; Shamir, U.; Marks, D.H. Water distribution reliability: Simulation methods. *J. Water Resour. Plan. Manag.* **1988**, *114*, 276–294. [CrossRef]
42. Tabucchi, T.; Davidson, R.; Brink, S. Simulation of post-earthquake water supply system restoration. *Civ. Eng. Environ. Syst.* **2010**, *27*, 263–279. [CrossRef]
43. Han, Z.; Ma, D.; Hou, B.; Wang, W. Seismic resilience enhancement of urban water distribution system using restoration priority of pipeline damages. *Sustainability* **2020**, *12*, 914. [CrossRef]
44. Isoyama, R.; Ishida, E.; Yune, K.; Shirozu, T. Seismic damage estimation procedure for water supply pipelines. In *Anti-Seismic Measures on Water Supply*; IWA Publishing: London, UK, 2000; Volume 18, pp. 63–68.
45. Zhao, S.J.; Xiong, L.Y.; Ren, A.Z. A spatial–temporal stochastic simulation of fire outbreaks following earthquake based on GIS. *J. Fire Sci.* **2006**, *24*, 313–339. [CrossRef]
46. Paez, D.; Filion, Y.; Castro-Gama, M.; Quintiliani, C.; Santopietro, S.; Sweetapple, C.; Meng, F.; Farmani, R.; Fu, G.; Butler, D.; et al. Battle of postdisaster response and restoration. *J. Water Resour. Plan. Manag.* **2020**, *146*, 04020067. [CrossRef]
47. Atashi, M.; Ziaei, A.N.; Khodashenas, S.R.; Farmani, R. Impact of isolation valves location on resilience of water distribution systems. *Urban Water J.* **2020**, *17*, 560–567. [CrossRef]
48. Yen, J.Y. Finding the K shortest loopless paths in a network. *Manag. Sci.* **1971**, *17*, 712–716. [CrossRef]
49. Mays, L.W. *Water Distribution Systems Handbook*; McGraw-Hill: New York, NY, USA, 2000.
50. *GB 5749-2022*; Standards for Drinking Water Quality. China Standards Press: Beijing, China, 2022.
51. *GB 50137-2011*; Code for Classification of Urban Land Use and Planning of Land Surface. China Planning Press: Beijing, China, 2011.
52. *GB 50974-2014*; Technical Code for Fire Protection Water Supply and Hydrant Systems. China Planning Press: Beijing, China, 2014.
53. Zhang, J.; Zhang, M.Y. Seismic robustness computational methodology of community building portfolio coupled with water supply network based on probability-cloud model. *Comput.-Aided Civ. Infrastruct. Eng.* **2024**, *39*, 1676–1698. [CrossRef]

54. Adachi, T.; Ellingwood, B.R. Serviceability assessment of a municipal water system under spatially correlated seismic intensities. *Comput.-Aided Civ. Infrastruct. Eng.* **2009**, *24*, 237–248. [CrossRef]
55. Mascheri, G.; Chieffo, N.; Tondini, N.; Pinto, C.; Lourenço, P.B. Assessing the cascading post-earthquake fire-risk scenario in urban centres. *Sustainability* **2024**, *16*, 9075. [CrossRef]

Disclaimer/Publisher's Note: The statements, opinions and data contained in all publications are solely those of the individual author(s) and contributor(s) and not of MDPI and/or the editor(s). MDPI and/or the editor(s) disclaim responsibility for any injury to people or property resulting from any ideas, methods, instructions or products referred to in the content.